3D-TOGO: Towards Text-Guided Cross-Category 3D Object Generation

Zutao Jiang[1 6 *], **Guangsong Lu**[2 *], **Xiaodan Liang**[3 4],
Jihua Zhu[1 †], **Wei Zhang**[2], **Xiaojun Chang**[5], **Hang Xu**[2 †]

[1] School of Software Engineering, Xi'an Jiaotong University [2] Huawei Noah's Ark Lab
[3] Sun Yat-sen University [4] MBZUAI [5] ReLER, AAII, University of Technology Sydney [6] PengCheng Laboratory
taozujiang@gmail.com, luguansong@huawei.com, xdliang328@gmail.com,
zhujh@xjtu.edu.cn, wz.zhang@huawei.com, xiaojun.chang@uts.edu.au, chromexbjxh@gmail.com

Abstract

Text-guided 3D object generation aims to generate 3D objects described by user-defined captions, which paves a flexible way to visualize what we imagined. Although some works have been devoted to solving this challenging task, these works either utilize some explicit 3D representations (e.g., mesh), which lack texture and require post-processing for rendering photo-realistic views; or require individual time-consuming optimization for every single case. Here, we make the first attempt to achieve generic text-guided cross-category 3D object generation via a new 3D-TOGO model, which integrates a text-to-views generation module and a views-to-3D generation module. The text-to-views generation module is designed to generate different views of the target 3D object given an input caption. *prior*-guidance, caption-guidance and view contrastive learning are proposed for achieving better view-consistency and caption similarity. Meanwhile, a pixelNeRF model is adopted for the views-to-3D generation module to obtain the implicit 3D neural representation from the previously-generated views. Our 3D-TOGO model generates 3D objects in the form of the neural radiance field with good texture and requires no time-cost optimization for every single caption. Besides, 3D-TOGO can control the category, color and shape of generated 3D objects with the input caption. Extensive experiments on the largest 3D object dataset (i.e., ABO) are conducted to verify that 3D-TOGO can better generate high-quality 3D objects according to the input captions across **98** different categories, in terms of PSNR, SSIM, LPIPS and CLIP-score, compared with text-NeRF and Dreamfields.

1 Introduction

Automatic 3D object generation has significant application values for many practical application scenarios, including games, movies, virtual reality, etc. In this paper, we study a challenging yet interesting and valuable task, called text-guided 3D object generation. With a text-guided 3D object generation model, one can give a textual description of their wanted 3D object, and leverage such a model to generate the corresponding 3D object, providing a flexible path for visualizing what we imagined.

---

[*]These authors contributed equally.
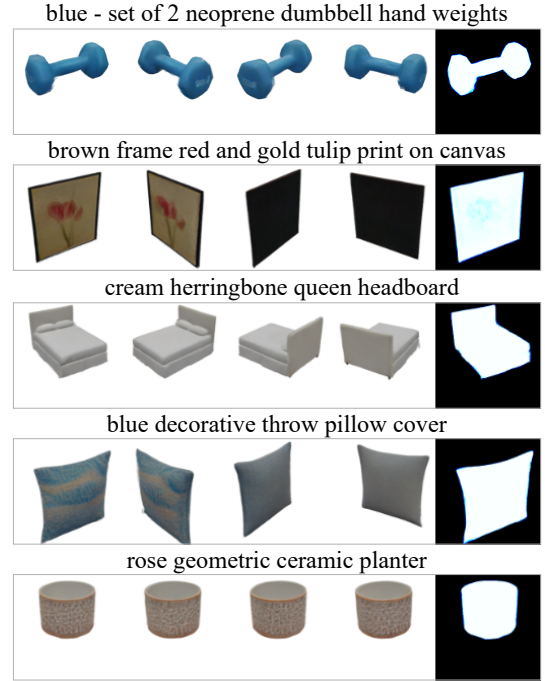
[†]Corresponding authors.

Figure 1: Generation results of our proposed 3D-TOGO model. For each case, we show the input caption, 4 rendered novel views of the generated 3D object and the transmittance from the first view. Transmittance represents how visible a point is from a particular view.

Along with the success of image generation models (Goodfellow et al. 2014; Vaswani et al. 2017; Ho, Jain, and Abbeel 2020), plenty of works have been devoted for text-to-image generation (Reed et al. 2016; Zhang et al. 2017, 2018a; Xu et al. 2018; Dong et al. 2017; Ramesh et al. 2021; Ding et al. 2021, 2022; Nichol et al. 2021; Ramesh et al. 2022), which shows appealing text-guided generation results. However, there are still few works for text-guided 3D object generation. Some prior works generate 3D shapes from natural language descriptions in the form of meshes (Michel et al. 2022), voxels (Chen et al. 2018), point clouds (Zhou, Du, and Wu 2021), and implicit functions (Liu et al. 2022). While they provide promising results, the

issue is that they require tedious post-processing steps, e.g. unwrapping a UV map in Blender, due to the lack of texture when used for multimedia applications. Recently, Neural Radiance Field (NeRF (Mildenhall et al. 2020)) has been successfully applied to the novel view synthesis task. Compared with other 3D representations, neural radiance fields can be sampled at high spatial resolutions and is easy to optimize. Empowered with the visual-language alignment capability of the pre-trained CLIP model, Dreamfields (Jain et al. 2022) leverages a given input text to guide the training of neural radiance fields. The shortcoming of Dreamfields is that it requires individually optimizing a network for each input text, which is time-consuming and computation expensive. Built on the disentangled conditional NeRF (Schwarz et al. 2020) and CLIP model, CLIP-NeRF (Wang et al. 2022) designs two code mappers to edit the shape and color of existing 3D objects with a text or image prompt. However, it only allows editing objects in the same category.

In this paper, we make the first attempt to achieve the generic text-guided **cross-category** 3D object generation and propose our 3D-TOGO model, standing on the progress of text-to-image generation models and Neural Radiance Fields. Our 3D-TOGO model consists of two modules: a) a view-consistent text-to-views generation module that generates views of the target 3D object given an input caption; b) a generic views-to-3D generation module for 3D object generation based on the previously-generated views. Specifically, we adopt the Transformer-based auto-regressive model (Vaswani et al. 2017) for our text-to-views generation module, because of its excellent cross-modal fusion capability. To complement the original token-level cross-entropy loss, we introduce the fine-grained pixel-level supervision signals for better view fidelity. We also incorporate caption-guidance by leveraging the visual-language alignment ability from CLIP (Radford et al. 2021) for better caption similarity. Furthermore, our text-to-views generation module achieves better view-consistency by conditioning on $prior$ view and adopting a novel view contrastive learning method. For the generic views-to-3D generation module, we follow the diagram of the previously-proposed pixelNeRF (Yu et al. 2021). As pixelNeRF optimizes neural radiance fields in the view space of the input image, so we can process each generated view independently and obtain an individual latent intermediate representation for each generated view, which can be aggregated across different views and generate the desired 3D neural representation matched with the input text. Besides, our views-to-3D generation module aims to learn scene prior instead of remembering the training dataset, allowing it to be used for generating objects across different categories.

We perform extensive experiments on the largest 3D object dataset ABO (Collins et al. 2022). Quantitative and qualitative comparisons against baseline methods, including text-NeRF and Dreamfields (Jain et al. 2022), show that our proposed 3D-TOGO model can better generate high-quality 3D objects according to the input captions across different object categories. Compared to baseline methods, the average CLIP-score of our model surpasses **4.4** on randomly selected text inputs, indicating better semantic consistency between the input captions and the generated 3D objects of our model. Besides, results from our 3D-TOGO model show that text-guided 3D object generation allows for flexible control over categories, colors and shapes. Our main contributions are summarized as follows:

- We make the first attempt to resolve the new text-guided cross-category 3D object generation problem and propose 3D-TOGO model, which has an efficient generation process requiring no inference time optimization.

- We propose a text-to-views generation module to generate consistent views given the input captions. We design $prior$-guidance to improve the consistency between adjacent views of a 3D object and introduce view contrastive learning to improve the consistency between different views of a 3D object. Caption-guidance is proposed for better caption similarity. Fine-grained pixel-level supervision is designed for better view fidelity.

- Our 3D-TOGO model can generate high-quality 3D objects across **98** categories. Besides, our 3D-TOGO model is empowered with the ability to control the **category**, **color** and **shape** according to the input caption.

2   Related Work

Text-to-Image Generation. Text-to-image generation focuses on generating images described by input captions. Based on the progresses on generative models, including generative adversarial networks (GANs (Goodfellow et al. 2014)), auto-regressive model (Vaswani et al. 2017) and diffusion model (Ho, Jain, and Abbeel 2020), there are numbers of works for text-to-image generation. Among them, many GAN-based models are proposed for better visual fidelity and caption similarity (Reed et al. 2016; Zhang et al. 2017, 2018a; Xu et al. 2018; Li et al. 2019a; Dong et al. 2017; Tao et al. 2020; Ye et al. 2021). However, GANs suffer from the well-known problem of mode-collapse and unstable training process. Besides GANs, another line of works explore applying Transformer-based auto-regressive model for text-to-image generation (Ramesh et al. 2021; Ding et al. 2021; Esser et al. 2021; Ding et al. 2022; Zhang et al. 2021; Lee et al. 2022). Recent works adopt diffusion model for text-to-image generation (Nichol et al. 2021; Ramesh et al. 2022). However, as the diffusion model predicts the added noise instead of the target images, it is complicated to apply constraints on the generated images. We adopt the architecture of Transformer (Vaswani et al. 2017) for our view-consistent text-to-views generation module, due to its high cross-modality fusion capability proven in the domain of multi-modal pre-training (Li et al. 2019b; Chen et al. 2020; Wang et al. 2021; Tan and Bansal 2019; Ni et al. 2021; Zhou et al. 2021; Zhuge et al. 2021) and generation mentioned above. Furthermore, we adopt the auto-regressive generation paradigm due to the aforementioned drawbacks of GANs and diffusion model.

Text-Guided 3D Object Generation. Compared with text-to-image generation, it is more challenging to generate 3D objects from the given text description. Some early works generate or edit 3D objects with a pre-trained CLIP model (Radford et al. 2021). Text2Mesh(Michel et al.

2022) edits the style of a 3D mesh by conforming the rendered images to a target text prompt with a CLIP-based semantic loss. It is tailored to a single mesh and could not generate 3D objects from scratch given a text prompt. (Khalid et al. 2022a) facilitates zero-shot text-driven mesh generation by deforming from a template mesh guided by CLIP. Text2shape (Chen et al. 2018) generates the voxelized objects using text-conditional Wasserstein GAN (Arjovsky, Chintala, and Bottou 2017), but only allows the 3D object generation of individual category and the performance is limited by the low-resolution 3D representation. CLIP-Forge (Sanghi et al. 2022) models the distribution of shape embeddings conditioned on the image features using a normalizing flow network during the training stage, and then conditions the normalizing flow network with text features to generate a shape embedding during the inference stage, which can be converted into a 3D shape via the shape decoder. However, their generated 3D objects lack color and texture and the quality of generated 3D objects is still limited, which is crucial for practical applications. Recently, (Liu et al. 2022) represents 3D shape with the implicit occupancy representation, which can be used to predict an occupancy field. They design a cyclic loss to encourage the consistency between the generated 3D shape and the input text. However, it cannot generate realistic 3D objects with high fidelity. There are also some works focus on 3D avatar generation and animation from text(Hong et al. 2022; Hu et al. 2021; Canfes et al. 2022), while our work focuses on 3D object generation from text. Compared with the above approaches, our 3D-TOGO model can generate high-quality 3D objects with color and texture across categories and requires no inference time optimization.

3 Method

Figure 2 shows the framework of our proposed 3D-TOGO model for text-guided 3D object generation. In this section, we will first introduce our view-consistent text-to-views generation module, which takes captions of 3D objects and different camera poses as input, enabling the multi-view image generation. Then we will introduce how to obtain the 3D implicit neural representation of the objects from the previously-generated views.

3.1 View-Consistent Text-to-Views Generation Module

Given an input caption t, our text-to-views generation module aims to generate 2D images $\{\hat{x}_i\}_{i=1}^N$ of different camera poses $\{\mathbf{P}_i\}_{i=1}^N$ for the corresponding 3D object described by caption t, where N is the number of generated views for a 3D object. $\{x_i\}_{i=1}^N$ denotes the ground truth images in dataset. The generated images $\hat{x}_i$ need to be consistent with its corresponding input caption t and camera pose $\mathbf{P}_i$. Besides, different views of the same input caption need to be view-consistent, i.e., images of different poses need to be consistent with each other as they are rendered from the same 3D object. For brevity, we omit the subscript of x, $\hat{x}$, and $\mathbf{P}$ in the rest of this section.

Base Text-to-Views Generation Module To generate images of different camera poses given an input caption, we start with designing our base generation module to generate image $\hat{x}$ conditioned on caption t and camera pose $\mathbf{P}$. We adopt the architecture of Transformer (Vaswani et al. 2017) due to its high cross-modality fusion capability (Li et al. 2019b; Wang et al. 2021; Ramesh et al. 2021; Ding et al. 2021; Lee et al. 2022). Following previous works, we transform camera pose $\mathbf{P}$, caption t and image x into sequences of tokens, and train a decoder-only Transformer model with a causal attention mask to predict the sequence of image tokens autoregressively conditioned on camera pose and caption tokens.

Specifically, our Transformer-based image generation module consists of an VQGAN (Esser, Rombach, and Ommer 2021) model, serving as an image tokenizer for quantizing the input image as discrete tokens and recovering the origin image from these discrete tokens, and a Transformer model for fitting the joint distribution of camera pose, caption and image tokens. The autoencoder model consists of an encoder E, a decoder G and a codebook $Z \in \mathbb{R}^{K \times n_z}$ containing K n_z-dimensional codes. Given an image $x \in \mathbb{R}^{H \times W \times 3}$, E first encodes the image into a two-dimensional feature map $\mathbf{F} \in \mathbb{R}^{h \times w \times n_z}$, and then the feature map $\mathbf{F}$ is quantized by replacing each pixel embedding with its closest code within the codebook element-wisely: $\hat{\mathbf{F}}_{ij} = \arg\min_{\mathbf{z}_k} \| \mathbf{F}_{ij} - \mathbf{z}_k \|^2$. The decoder G is for taking the quantized feature map $\hat{\mathbf{F}}$ as input and reconstructing an pixel-level image $\hat{x}$ close to the original image x, i.e., $\hat{x} \approx x$. With the aforementioned image tokenizer, image x can be tokenized as a sequence of discrete tokens $\{\mathbf{I}_i\}_{i=1}^{N_\mathbf{I}}$. Meanwhile, caption t is encoded into sequence of discrete tokens $\{\mathbf{T}_i\}_{i=1}^{N_\mathbf{T}}$ with a Byte-Pair Encoding (BPE (Sennrich, Haddow, and Birch 2015)) tokenizer. $N_\mathbf{I}$ and $N_\mathbf{T}$ denotes the length of image token sequence and caption token sequence respectively. For camera pose $\mathbf{P}$, we select $N_\mathbf{P}$ poses across different objects so that each camera pose is correspond to an unique token denoted as $\mathbf{V}$. The Transformer is trained to predict the sequence of $[\mathbf{V}, \{\mathbf{T}_i\}_{i=1}^{N_\mathbf{T}}, \{\mathbf{I}_i\}_{i=1}^{N_\mathbf{I}}]$ auto-regressively, which minimizes cross entropy losses applied to the predicted tokens of camera pose, text and image, respectively as follows: $\mathcal{L}_{pose} = CE(\hat{\mathbf{V}}, \mathbf{V})$, $\mathcal{L}_{txt} = \mathbb{E}_i[CE(\hat{\mathbf{T}}_i, \mathbf{T}_i)]$, $\mathcal{L}_{img} = \mathbb{E}_i[CE(\hat{\mathbf{I}}_i, \mathbf{I}_i)]$, where $\hat{\mathbf{V}}$, $\hat{\mathbf{T}}_i$ and $\hat{\mathbf{I}}_i$ are the predicted tokens of camera pose, caption and image respectively; $\mathbb{E}_i[\cdot]$ denotes the expectation and CE represents cross-entropy loss.

Pixel-Level Supervision and Caption-Guidance One shortage of the aforementioned base text-to-views generation module is that the training loss is applied on image tokens, lacking fine-grained pixel-level supervision signals and leading to low visual quality. To this end, to complement such token-level loss, we explore some pixel-level supervision signals applied on the generated image $\hat{x}$ (decoded from the generated image tokens $\{\hat{\mathbf{I}}_i\}_{i=1}^{N_\mathbf{I}}$ with the image tokenizer) for more fine-grained supervision signals and better image fidelity. We first explore training losses between the original image x and generated image $\hat{x}$. In our preliminary
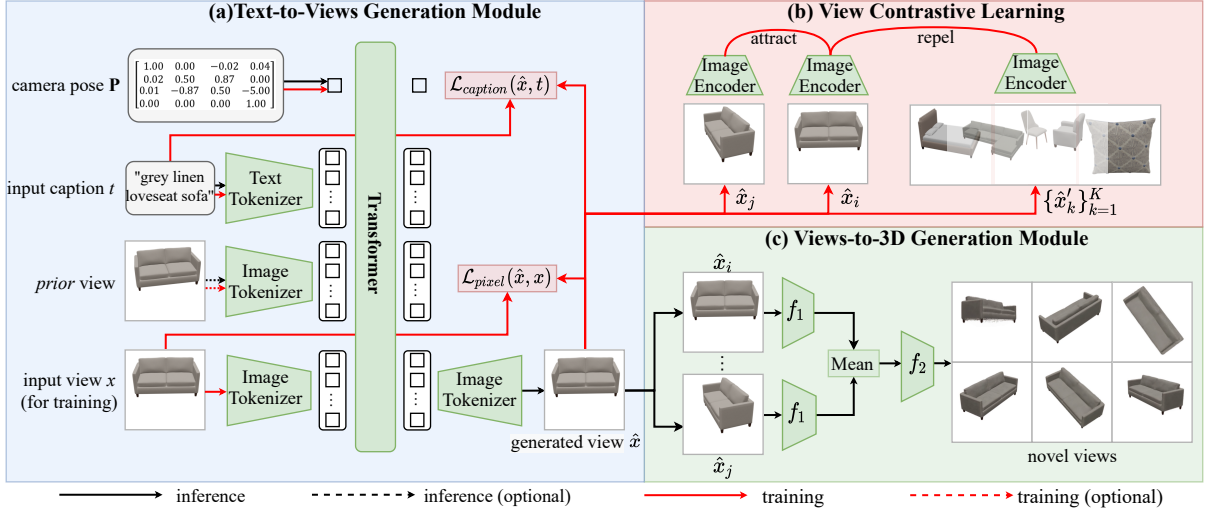
Figure 2: The framework of our 3D-TOGO model for text-guided 3D object generation. (a) Text-to-views generation module. Fine-grained pixel-level supervision signal $\mathcal{L}_{pixel}$ and caption-guidance loss $\mathcal{L}_{caption}$ are for better view fidelity and caption similarity. (b) View contrastive learning for better view-consistency. (c) Views-to-3D generation module. It takes the previously-generated views as input and generates the implicit 3D neural representation, from which novel views can be obtained.

experiments, we tried $L1$ loss and Perceptual loss (Johnson, Alahi, and Fei-Fei 2016). Similar results are observed so that we use the simpler $L1$ loss as: $\mathcal{L}_{pixel} = L1(\hat{x}, x)$. Gradient back-propagation from the generated image $\hat{x}$ to the generated image tokens $\{\hat{\mathbf{I}}_i\}_{i=1}^{N_{\mathbf{I}}}$ is implemented with straight-through estimator (Bengio, Léonard, and Courville 2013).

Besides, we explore some supervision signals applied between the generated image $\hat{x}$ and input caption t, called caption-guidance, for better caption similarity, i.e., the generated images better match the semantics of the input captions. To this end, we explore leveraging the power of the CLIP model (Radford et al. 2021), which is pre-trained with 400 million image-text pairs collected from the Web and shows excellent zero-shot visual-language alignment capability. Specifically, we utilize the pre-trained ViT-B/32 CLIP model to calculate the similarity score between the generated image $\hat{x}$ and input caption t and apply a caption-guidance loss as: $\mathcal{L}_{caption} = -Sim_{CLIP}(\hat{x}, t)$, to enforce the generation module to generate images that are more semantically similar to the input caption.

***prior*-Guidance and View Contrastive Learning** Until now, it is still challenging for the text-to-views generation module to generate view-consistent images among different camera poses, as it is (1) trained to generate images conditioned on only camera pose and caption, without information from images of other poses, (2) without any view-consistency supervision signal during training.

To improve the consistency between adjacent views, we first propose to condition the generation module on a piece of extra information: an image of another camera pose, which we call *prior* view. To this end, we specify a fixed order of different camera poses and condition image generation of the current camera pose on the previous one. During training, such *prior* view is masked half of the time so that the generation module is able to perform image gener-

ation with and without *prior* view. During inference, given an input caption t, the first view is generated without *prior* view, while the others are generated using the previously generated one as *prior* view one by one in order. Tokens of input *prior* view and predicted *prior* view are denoted as $\{\mathbf{I}_i^{prior}\}_{i=1}^{N_{\mathbf{I}}}$ and $\{\hat{\mathbf{I}}_i^{prior}\}_{i=1}^{N_{\mathbf{I}}}$ respectively. A reconstruction loss is also applied on the predicted *prior* view tokens as: $\mathcal{L}_{prior} = \mathbb{E}_i \, CE(\hat{\mathbf{I}}_i^{prior}, \mathbf{I}_i^{prior})$.

Furthermore, we incorporate the concept of contrastive learning for better view-consistency. In our case, as we can see, different views of the corresponding object of an input caption should be closer to each other, than to views of the corresponding object of a different input caption. This is the same as the objective of contrastive learning. To this end, we propose view contrastive learning, where views of the same object are treated as positive samples of each other, while views of different objects are treated as negative samples of each other. During training, we generate two different views $\hat{x}_i$, $\hat{x}_j$, $i \neq j$ of the same object, and a set of K views $X = \{\hat{x}'_1, \hat{x}'_2, ..., \hat{x}'_K\}$ of different objects. Besides, we learn an image encoder f_{enc} for extracting view representations $f_{enc}(x)$. Then the objective function of view contrastive learning can be formulated as follows:

$$\mathcal{L}_{contrastive} = -\log \frac{\exp(sim(f_{enc}(\hat{x}_i), f_{enc}(\hat{x}_j))/\tau)}{\sum_{x \in X} \exp(sim(f_{enc}(\hat{x}_i), f_{enc}(x))/\tau)}, \quad (1)$$

where $sim(\cdot, \cdot)$ denotes cosine similarity and τ denotes a temperature parameter.

Finally, the overall objective function of our view-consistent text-to-views generation module is as follows:

$$\begin{aligned}\mathcal{L} = &\lambda_{pose}\mathcal{L}_{pose} + \lambda_{txt}\mathcal{L}_{txt} \\ &+ \lambda_{prior}\mathcal{L}_{prior} + \lambda_{img}\mathcal{L}_{img} + \lambda_{pixel}\mathcal{L}_{pixel} \quad (2) \\ &+ \lambda_{caption}\mathcal{L}_{caption} + \lambda_{contrastive}\mathcal{L}_{contrastive},\end{aligned}$$

where λ_{pose}, λ_{txt}, λ_{prior}, λ_{img}, λ_{pixel}, $\lambda_{caption}$ and $\lambda_{contrastive}$ are the balancing coefficients.

3.2 Views-to-3D Generation Module

Given images $\hat{\mathscr{I}} = \{\hat{x}_i\}_{i=1}^N$ generated by the text-to-views module, the aim of views-to-3D module is to obtain the implicit neural representation of the generated 3D object, where N is the number of generated images. In experiments, we find that NeRF (Mildenhall et al. 2020) fails to obtain high-quality novel view synthesis results in some cases, if we naively optimize NeRF with the generated images. This is because that there are still some small inconsistent contents among the generated images. Therefore, we introduce pixelNeRF (Yu et al. 2021) to firstly learn scene prior from the ground-truth images $\mathscr{I} = \{x_i\}_{i=1}^M$ across objects in the training data, where $M(M \geq N)$ is the number of rendered images of 3D objects. Please refer to (Yu et al. 2021) regarding the network architecture details of pixelNeRF model.

Once obtaining the scene prior, we can encode the generated 3D object as a continuous volumetric radiance field f of color c and density σ by using the generated multi-view images $\hat{\mathscr{I}}$. Similar to pixelNeRF, we use the view space of the generated images instead of the canonical space. Specially, for a 3D query point y in the neural radiance fields, we first retrieve the corresponding image features from $\hat{\mathscr{I}}$ by $\{w_i\}_{i=1}^N = \{\mathbf{W}_i(\pi_i(y))\}_{i=1}^N$, where $\mathbf{W}_i = E(\hat{x}_i)$ is the feature volume extracted from the generated image $\hat{x}_i$, $\pi_i(y)$ denotes the corresponding image coordinate on the image plane of the generated image $\hat{x}_i$, and $\mathrm{W}_i(\pi_i(y))$ represents the image feature extracted from feature volume W_i for the 3D query point y.

Then, we need to obtain the intermediate representation $U = \{U_i\}_{i=1}^N$ in each view space of the generated images $\hat{\mathscr{I}}$ for query point y with view direction d as follows:

$$U_i = f_1(\gamma(\mathbf{H}(y)_i), d_i; w_i), \qquad (3)$$

where $\mathbf{H}(y)_i = \mathbf{P}_i y = \mathbf{R}_i y + h_i$ denotes that transforming the query point y into the coordinate system of the generated image $\hat{x}_i$, $\mathbf{P}_i$ is the world to camera transformation matrix, $\mathbf{R}_i$ is the rotation matrix, h_i is the translation vector, $\gamma(\cdot)$ represents a positional encoding on the transformed query point $\mathbf{H}(y)_i$ with 6 exponentially increasing frequencies (Mildenhall et al. 2020); $d_i = \mathbf{R}_i d$ denotes transforming the view direction d into the coordinate system of the generate image $\hat{x}_i$; w_i is the corresponding image feature extracted from the generate image $\hat{x}_i$; $f_1(\cdot)$ represents the layers of the pixelNeRF to process transformed query point, transformed view direction and the corresponding extracted image feature in the view space of the generated images $\hat{\mathscr{I}}$ independently, which has been trained on the ABO training dataset.

After obtaining all the intermediate representation $U = \{U_i\}_{i=1}^N$, we use the average pooling operator η to aggregate them and then pass the layers of the pixelNeRF to process the aggregated representation. This process can be written as:

$$f(y, d) = (\sigma(y), c(y, d)) = f_2(\eta(U_i))_{i=1}^N, \qquad (4)$$

where f_2 denotes the layers to process the aggregated representation $\eta(U_i)_{i=1}^N$, $\sigma(y)$ is the density of the 3D query point y which is independent of the view direction d, $c(y, d)$ represents the color of the 3D query point y in the view direction d, $f(\cdot)$ is the final continuous volumetric radiance field which representing the generated 3D object matched with the input caption t. For the photo-realistic rendering of the generated 3D object, we use the volume rendering technique proposed in (Mildenhall et al. 2020).

4 Experiments

Dataset. Our approach is evaluated on Amazon-Berkeley Objects (ABO) (Collins et al. 2022), a large-scale dataset containing nearly **8,000** real household objects from **98** categories with their corresponding nature language descriptions. We use ABO dataset because it contains the categories of other small datasets, such as ShapeNet(Chen et al. 2018). Benefiting from their detailed texture and non-lambertian BRDFs, the 3D models in ABO can be photo-realistically rendered. To construct multi-view images dataset with their nature language descriptions, we use Blender (Community 2018) to render each 3D model into 256×256 RGB-alpha images from 36 cameras. Camera elevation is set as $-30°$ and camera azimuth is sampled uniformly from the range $[-180°, 180°]$. Totally, 286,308 multi-view images are rendered from 7,953 objects belong to 98 categories. We randomly split 80%, 10%, 10% objects as our training, validation, and test set, respectively.

Metrics. Following the settings of (Yu et al. 2021), we evaluate the quality of our generated 3D objects by measuring the quality of novel view synthesis. Specifically, PSNR, SSIM(Wang et al. 2004), LPIPS (Zhang et al. 2018b) are adopted as our metrics. We also compute the CLIP score (Radford et al. 2021) between the rendered novel view images and the corresponding natural language description, which can measure the semantic consistency of the generated 3D objects with the description. The ResNet-50 CLIP model is adopted. Besides, we also adopt human evaluation for comparison. Two metrics are considered: **object fidelity** (including view fidelity and consistency among different views) and **caption similarity**. For each input caption, results from different methods are shown in random order and the workers are asked to order different results in terms of these two metrics. The average rank from different workers is used as the final score. 94 human evaluation results are collected. The higher PSNR, SSIM and CLIP score, the better; the lower LPIPS, object fidelity and caption similarity, the better.

Experimental Setup. We implement our algorithm with Pytorch. The hyper-parameters of λ_{pose}, λ_{txt}, λ_{prior}, λ_{img}, λ_{pixel}, $\lambda_{caption}$ and $\lambda_{contrastive}$ are set to 0.1, 0.1, 0.1, 0.6, 1, 1 and 1 respectively. For our text-to-views generation module, we use AdamW optimizer to train 20 epochs. For the views-to-3D generation module, we use Adam optimizer to train 100 epochs and randomly select 9 views during each training step. More details are provided in the Appendix.

4.1 Comparison Against Baselines

As our 3D-TOGO model generates objects in the form of neural radiance fields, so we select two NeRF-based

Table 1: Quantitative comparison against text-NeRF (short for text-to-views generation + NeRF(Mildenhall et al. 2020)) and Dreamfields (Jain et al. 2022).

| Metric	Method	text1	text2	text3	text4	text5	text6	12 Texts Avg.
PSNR ↑	text-NeRF	18.15	19.96	0.79	22.02	18.12	0.48	14.04
	Ours	**20.12**	**23.34**	**26.41**	**24.02**	**23.80**	**26.53**	**24.98**
SSIM ↑	text-NeRF	0.856	0.898	0.001	0.876	0.863	0.001	0.636
	Ours	**0.889**	**0.920**	**0.925**	**0.898**	**0.897**	**0.864**	**0.900**
LPIPS ↓	text-NeRF	0.138	0.091	0.503	0.142	0.167	0.475	0.239
	Ours	**0.122**	**0.063**	**0.075**	**0.128**	**0.165**	**0.082**	**0.092**
CLIP- Score ↑	Dreamfields	18.92	21.34	18.13	16.31	18.08	18.73	18.40
	text-NeRF	26.65	20.28	13.90	21.12	23.16	11.84	18.38
	Ours	**27.08**	**22.67**	**20.98**	**22.74**	**24.13**	**25.08**	**22.84**
Object Fidelity ↓	Dreamfields	3.00	2.56	2.04	2.94	2.94	1.94	2.63
	text-NeRF	1.97	2.32	2.93	2.04	1.97	2.95	2.27
	Ours	**1.03**	**1.12**	**1.03**	**1.02**	**1.09**	**1.12**	**1.11**
Caption Similarity ↓	Dreamfields	2.97	2.66	2.02	2.94	2.87	2.01	2.64
	text-NeRF	1.98	2.19	2.95	2.03	1.97	2.95	2.25
	Ours	**1.05**	**1.15**	**1.03**	**1.03**	**1.16**	**1.04**	**1.11**
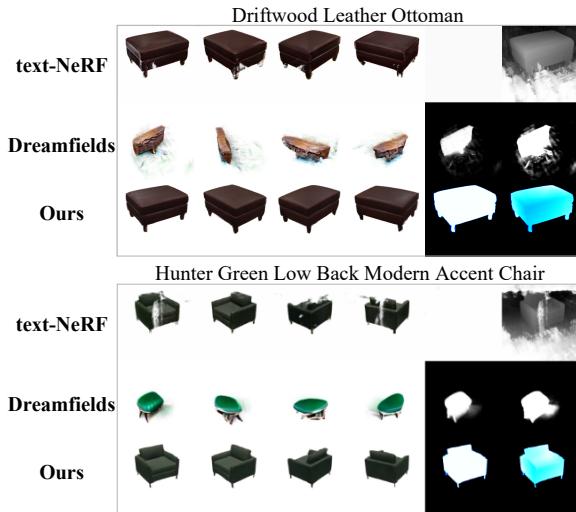
Figure 3: Visual comparison against two baseline methods. For each sub figure, the textual title is the input caption, and the first 4 images are rendered novel views of the generated 3D object while the last two images are transmittance and depth from the first view respectively.

text-guided 3D object generation methods as our baseline: text-to-views generation module + NeRF (Mildenhall et al. 2020) (called text-NeRF for convenient in the following) and Dreamfields (Jain et al. 2022). We use the code open-sourced by the authors. As both text-NeRF and Dreamfields require training an individual network for each given natural language description, we randomly select 12 text descriptions from our test set as the input captions. The selected text descriptions are included in the Appendix. As there is no ground truth for the generated views of Dreamfields, we do not use PSNR, SSIM and LPIPS in the comparison against Dreamfields.

Table 1 shows the quantitative comparison among different methods. Results of the first 6 descriptions and the average of 12 descriptions are shown while results of the rest 6 text descriptions are included in the Appendix. As we can see, for all cases, 3D-TOGO achieves the best results. Additionally, Figure 3 shows the qualitative comparison among different methods. Results of the first 2 descriptions are shown while results of the rest 10 descriptions are included in the Appendix. As we can see, text-NeRF generates broken objects, as there are still some small inconsistent contents among the generated images. Figure 3 shows that Dreamfields cannot generate reasonable results. This may be because Dreamfields cannot generalize to household objects or it requires attentive hyperparameter-tuning. Besides, both text-NeRF and Dreamfields require time-consuming per-case optimization, while 3D-TOGO can be used across objects.

4.2 Text-Guided 3D Object Generation

Figure 1 shows the cross-category text-guided 3D generation results of our proposed 3D-TOGO model. Our model generates high-fidelity 3D objects matching the input caption across different object categories. Besides, Figure 4 shows that our method can control the color and shape of the generated 3D objects by the input caption flexibly. More results are included in the Appendix.

4.3 Ablation Study

In this section, we first study the effectiveness of different objectives on the quality of generated views from the text-to-views generation module and 3D objects from the views-to-3D generation module respectively. For quantitative comparison of the quality of generated views, we adopt metrics including FID (Heusel et al. 2017), KID (Bińkowski et al. 2018), CLIP score and consistency error. Consistency error
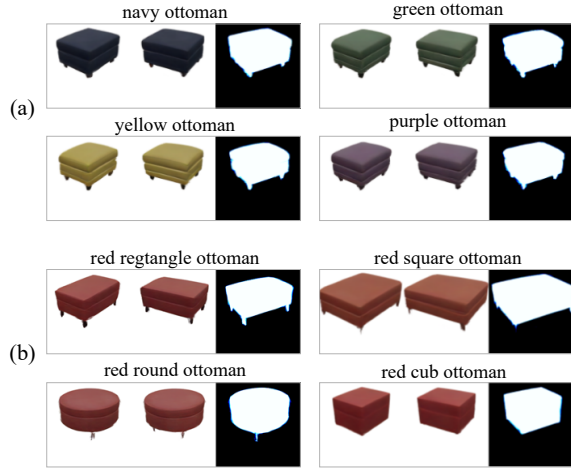
Figure 4: 3D object generation results with controlled (a) color and (b) shape. For each case, we show the input caption, 2 rendered novel views of the generated 3D object and the transmittance from the first view.

Table 2: Ablation study of our text-to-views generation module. '*prior*', 'contrastive', 'caption' and 'L1' indicates *prior*-guidance, view contrastive learning, caption-guidance and pixel-level L1 loss respectively.

prior	contrastive	caption	L1	consistency-error ↓
				9.47
✓				8.88
	✓			9.17
		✓		9.23
			✓	9.35
✓	✓			8.61
✓		✓		8.81
✓		✓	✓	8.74
✓	✓	✓	✓	**8.56**
		GT		7.55

measures the average L2 error between views of adjacent camera poses and reflects view consistency to some degree. The lower the consistency error, the better view consistency. Results of consistency error are shown in Table 2 while results of FID, KID, and CLIP-score are included in the Appendix. Then we study the effect of the number of views N used for the views-to-3D generation module.

View Generation Quality. Table 2 shows the quantitative results of our text-to-views generation module. As we can see, *prior*-guidance improves the consistency-error from 9.47 to 8.88, and view contrastive learning further improves it to 8.61, indicating both of these two improvements contribute to improving view-consistency. Besides, our complete text-to-views generation module achieves the best consistency-error of 8.56.

3D Object Generation Quality. Table 3 shows the CLIP-scores of our views-to-3D generation module for different object categories. The detailed results for each category will be provided in the Appendix. As we can see, 3D object generation based on the results of our complete text-to-

Table 3: Ablation study of our text-to-views generation module and the effectiveness on 3D object generation.

prior	contrastive	caption	L1	CLIP-score ↑
				19.91
✓				20.50
	✓			19.97
		✓		20.14
			✓	19.99
✓	✓			20.54
✓		✓		20.90
✓		✓	✓	20.93
✓	✓	✓	✓	**21.01**

Table 4: Ablation study results on the ABO test set regarding the number of views N.

#	PSNR ↑	SSIM ↑	LPIPS ↓	CLIP-score ↑
1	9.69	0.512	0.540	12.99
3	18.57	0.800	0.240	16.36
6	21.00	0.868	0.137	20.52
9	21.18	0.873	**0.133**	**20.71**
18	**21.30**	**0.877**	**0.133**	20.54

views generation module achieves the best CLIP-score in all shown categories and achieves the best average CLIP-score among all categories of the ABO test set.

Number of views N**.** Table 4 shows the quantitative results of different number of views N used for views-to-3D generation module. We evaluate the quality of generated 3D objects by measuring the quality of novel view synthesis. As we can see, more views yield better results in general. 9 views yield similar results to 18 views, so we set $N = 9$ in our aforementioned experiments.

5 Conclusion

In this paper, we propose the 3D-TOGO model for the first attempt to achieve the generic text-guided 3D object generation. Our 3D-TOGO integrates a view-consistent text-to-views generation module for generating views of the target 3D object given an input caption; and a generic cross-scene neural rendering module for 3D object generation. For the text-to-views generation module, we adopt fine-grained pixel-level supervision signals, *prior*-guidance, caption-guidance and view contrastive learning for achieving better view fidelity, view-consistency and caption similarity. A pixelNeRF model is adopted for the generic implicit 3D neural representation synthesis module. Extensive experiments on the largest 3D object dataset ABO show that our proposed 3D-TOGO model can better generate high-quality 3D objects according to the input captions across 98 different object categories both quantitatively and qualitatively, compared against text-NeRF and Dreamfields (Jain et al. 2022). Our 3D-TOGO model also allows for flexible control over categories, colors and shapes with the input caption. We describe the potential negative societal impacts and limitations of our work in the Appendix.

References

Arjovsky, M.; Chintala, S.; and Bottou, L. 2017. Wasserstein generative adversarial networks. In *International conference on machine learning*, 214–223. PMLR.

Bengio, Y.; Léonard, N.; and Courville, A. 2013. Estimating or propagating gradients through stochastic neurons for conditional computation. *arXiv preprint arXiv:1308.3432*.

Bińkowski, M.; Sutherland, D. J.; Arbel, M.; and Gretton, A. 2018. Demystifying mmd gans. *arXiv preprint arXiv:1801.01401*.

Canfes, Z.; Atasoy, M. F.; Dirik, A.; and Yanardag, P. 2022. Text and Image Guided 3D Avatar Generation and Manipulation. *arXiv preprint arXiv:2202.06079*.

Chen, K.; Choy, C. B.; Savva, M.; Chang, A. X.; Funkhouser, T.; and Savarese, S. 2018. Text2shape: Generating shapes from natural language by learning joint embeddings. In *Asian conference on computer vision*, 100–116. Springer.

Chen, Y.-C.; Li, L.; Yu, L.; El Kholy, A.; Ahmed, F.; Gan, Z.; Cheng, Y.; and Liu, J. 2020. Uniter: Universal image-text representation learning. In *European conference on computer vision*, 104–120. Springer.

Collins, J.; Goel, S.; Deng, K.; Luthra, A.; Xu, L.; Gundogdu, E.; Zhang, X.; Vicente, T. F. Y.; Dideriksen, T.; Arora, H.; et al. 2022. Abo: Dataset and benchmarks for real-world 3d object understanding. In *Proceedings of the IEEE/CVF Conference on Computer Vision and Pattern Recognition*, 21126–21136.

Community, B. O. 2018. Blender - a 3D modelling and rendering package. *Blender Foundation, Stichting Blender Foundation, Amsterdam*.

Ding, M.; Yang, Z.; Hong, W.; Zheng, W.; Zhou, C.; Yin, D.; Lin, J.; Zou, X.; Shao, Z.; Yang, H.; et al. 2021. Cogview: Mastering text-to-image generation via transformers. *Advances in Neural Information Processing Systems*, 34: 19822–19835.

Ding, M.; Zheng, W.; Hong, W.; and Tang, J. 2022. CogView2: Faster and Better Text-to-Image Generation via Hierarchical Transformers. *arXiv preprint arXiv:2204.14217*.

Dong, H.; Yu, S.; Wu, C.; and Guo, Y. 2017. Semantic image synthesis via adversarial learning. In *Proceedings of the IEEE International Conference on Computer Vision*, 5706–5714.

Esser, P.; Rombach, R.; Blattmann, A.; and Ommer, B. 2021. Imagebart: Bidirectional context with multinomial diffusion for autoregressive image synthesis. *Advances in Neural Information Processing Systems*, 34: 3518–3532.

Esser, P.; Rombach, R.; and Ommer, B. 2021. Taming transformers for high-resolution image synthesis. In *Proceedings of the IEEE/CVF Conference on Computer Vision and Pattern Recognition*, 12873–12883.

Goodfellow, I.; Pouget-Abadie, J.; Mirza, M.; Xu, B.; Warde-Farley, D.; Ozair, S.; Courville, A.; and Bengio, Y. 2014. Generative adversarial nets. *Advances in neural information processing systems*, 27.

Heusel, M.; Ramsauer, H.; Unterthiner, T.; Nessler, B.; and Hochreiter, S. 2017. Gans trained by a two time-scale update rule converge to a local nash equilibrium. *Advances in neural information processing systems*, 30.

Ho, J.; Jain, A.; and Abbeel, P. 2020. Denoising diffusion probabilistic models. *Advances in Neural Information Processing Systems*, 33: 6840–6851.

Hong, F.; Zhang, M.; Pan, L.; Cai, Z.; Yang, L.; and Liu, Z. 2022. AvatarCLIP: Zero-Shot Text-Driven Generation and Animation of 3D Avatars. *ACM Transactions on Graphics (TOG)*, 41(4): 1–19.

Hu, L.; Qi, J.; Zhang, B.; Pan, P.; and Xu, Y. 2021. Text-driven 3D Avatar Animation with Emotional and Expressive Behaviors. In *Proceedings of the 29th ACM International Conference on Multimedia*, 2816–2818.

Jain, A.; Mildenhall, B.; Barron, J. T.; Abbeel, P.; and Poole, B. 2022. Zero-shot text-guided object generation with dream fields. In *Proceedings of the IEEE/CVF Conference on Computer Vision and Pattern Recognition*, 867–876.

Johnson, J.; Alahi, A.; and Fei-Fei, L. 2016. Perceptual losses for real-time style transfer and super-resolution. In *European conference on computer vision*, 694–711. Springer.

Khalid, N.; Xie, T.; Belilovsky, E.; and Popa, T. 2022a. Text to Mesh Without 3D Supervision Using Limit Subdivision. *arXiv preprint arXiv:2203.13333*.

Khalid, N. M.; Xie, T.; Belilovsky, E.; and Tiberiu, P. 2022b. Clip-mesh: Generating textured meshes from text using pretrained image-text models. *ACM Transactions on Graphics (TOG), Proc. SIGGRAPH Asia*.

Lee, D.; Kim, C.; Kim, S.; Cho, M.; and Han, W.-S. 2022. Autoregressive Image Generation using Residual Quantization. In *Proceedings of the IEEE/CVF Conference on Computer Vision and Pattern Recognition*, 11523–11532.

Li, B.; Qi, X.; Lukasiewicz, T.; and Torr, P. H. 2019a. Controllable text-to-image generation. In *Proceedings of the 33rd International Conference on Neural Information Processing Systems*, 2065–2075.

Li, L. H.; Yatskar, M.; Yin, D.; Hsieh, C.-J.; and Chang, K.-W. 2019b. Visualbert: A simple and performant baseline for vision and language. Preprint arXiv:1908.03557.

Liu, Z.; Wang, Y.; Qi, X.; and Fu, C.-W. 2022. Towards Implicit Text-Guided 3D Shape Generation. In *Proceedings of the IEEE/CVF Conference on Computer Vision and Pattern Recognition*, 17896–17906.

Michel, O.; Bar-On, R.; Liu, R.; Benaim, S.; and Hanocka, R. 2022. Text2mesh: Text-driven neural stylization for meshes. In *Proceedings of the IEEE/CVF Conference on Computer Vision and Pattern Recognition*, 13492–13502.

Mildenhall, B.; Srinivasan, P. P.; Tancik, M.; Barron, J. T.; Ramamoorthi, R.; and Ng, R. 2020. Nerf: Representing scenes as neural radiance fields for view synthesis. In *European conference on computer vision*, 405–421. Springer.

Ni, M.; Huang, H.; Su, L.; Cui, E.; Bharti, T.; Wang, L.; Zhang, D.; and Duan, N. 2021. M3p: Learning universal

representations via multitask multilingual multimodal pre-training. In *Proceedings of the IEEE/CVF Conference on Computer Vision and Pattern Recognition*, 3977–3986.

Nichol, A.; Dhariwal, P.; Ramesh, A.; Shyam, P.; Mishkin, P.; McGrew, B.; Sutskever, I.; and Chen, M. 2021. Glide: Towards photorealistic image generation and editing with text-guided diffusion models. *arXiv preprint arXiv:2112.10741*.

Poole, B.; Jain, A.; Barron, J. T.; and Mildenhall, B. 2022. Dreamfusion: Text-to-3d using 2d diffusion. *arXiv preprint arXiv:2209.14988*.

Radford, A.; Kim, J. W.; Hallacy, C.; Ramesh, A.; Goh, G.; Agarwal, S.; Sastry, G.; Askell, A.; Mishkin, P.; Clark, J.; et al. 2021. Learning transferable visual models from natural language supervision. In *International Conference on Machine Learning*, 8748–8763. PMLR.

Ramesh, A.; Dhariwal, P.; Nichol, A.; Chu, C.; and Chen, M. 2022. Hierarchical text-conditional image generation with clip latents. *arXiv preprint arXiv:2204.06125*.

Ramesh, A.; Pavlov, M.; Goh, G.; Gray, S.; Voss, C.; Radford, A.; Chen, M.; and Sutskever, I. 2021. Zero-shot text-to-image generation. In *International Conference on Machine Learning*, 8821–8831. PMLR.

Reed, S.; Akata, Z.; Yan, X.; Logeswaran, L.; Schiele, B.; and Lee, H. 2016. Generative adversarial text to image synthesis. In *International Conference on Machine Learning*, 1060–1069. PMLR.

Reizenstein, J.; Shapovalov, R.; Henzler, P.; Sbordone, L.; Labatut, P.; and Novotny, D. 2021. Common objects in 3d: Large-scale learning and evaluation of real-life 3d category reconstruction. In *Proceedings of the IEEE/CVF International Conference on Computer Vision*, 10901–10911.

Sanghi, A.; Chu, H.; Lambourne, J. G.; Wang, Y.; Cheng, C.-Y.; Fumero, M.; and Malekshan, K. R. 2022. Clip-forge: Towards zero-shot text-to-shape generation. In *Proceedings of the IEEE/CVF Conference on Computer Vision and Pattern Recognition*, 18603–18613.

Schwarz, K.; Liao, Y.; Niemeyer, M.; and Geiger, A. 2020. Graf: Generative radiance fields for 3d-aware image synthesis. *Advances in Neural Information Processing Systems*, 33: 20154–20166.

Sennrich, R.; Haddow, B.; and Birch, A. 2015. Neural machine translation of rare words with subword units. *arXiv preprint arXiv:1508.07909*.

Tan, H.; and Bansal, M. 2019. Lxmert: Learning cross-modality encoder representations from transformers. *arXiv preprint arXiv:1908.07490*.

Tao, M.; Tang, H.; Wu, S.; Sebe, N.; Jing, X.-Y.; Wu, F.; and Bao, B. 2020. Df-gan: Deep fusion generative adversarial networks for text-to-image synthesis. *arXiv preprint arXiv:2008.05865*.

Vaswani, A.; Shazeer, N.; Parmar, N.; Uszkoreit, J.; Jones, L.; Gomez, A. N.; Kaiser, Ł.; and Polosukhin, I. 2017. Attention is all you need. In *Advances in neural information processing systems*, 5998–6008.

Wang, C.; Chai, M.; He, M.; Chen, D.; and Liao, J. 2022. Clip-nerf: Text-and-image driven manipulation of neural radiance fields. In *Proceedings of the IEEE/CVF Conference on Computer Vision and Pattern Recognition*, 3835–3844.

Wang, Z.; Bovik, A. C.; Sheikh, H. R.; and Simoncelli, E. P. 2004. Image quality assessment: from error visibility to structural similarity. *IEEE transactions on image processing*, 13(4): 600–612.

Wang, Z.; Yu, J.; Yu, A. W.; Dai, Z.; Tsvetkov, Y.; and Cao, Y. 2021. SimVLM: Simple Visual Language Model Pre-training with Weak Supervision. Preprint arXiv:2108.10904.

Xu, T.; Zhang, P.; Huang, Q.; Zhang, H.; Gan, Z.; Huang, X.; and He, X. 2018. Attngan: Fine-grained text to image generation with attentional generative adversarial networks. In *Proceedings of the IEEE conference on computer vision and pattern recognition*, 1316–1324.

Ye, H.; Yang, X.; Takac, M.; Sunderraman, R.; and Ji, S. 2021. Improving text-to-image synthesis using contrastive learning. *arXiv preprint arXiv:2107.02423*.

Yu, A.; Ye, V.; Tancik, M.; and Kanazawa, A. 2021. pixelnerf: Neural radiance fields from one or few images. In *Proceedings of the IEEE/CVF Conference on Computer Vision and Pattern Recognition*, 4578–4587.

Zhang, H.; Xu, T.; Li, H.; Zhang, S.; Wang, X.; Huang, X.; and Metaxas, D. N. 2017. Stackgan: Text to photo-realistic image synthesis with stacked generative adversarial networks. In *Proceedings of the IEEE international conference on computer vision*, 5907–5915.

Zhang, H.; Xu, T.; Li, H.; Zhang, S.; Wang, X.; Huang, X.; and Metaxas, D. N. 2018a. Stackgan++: Realistic image synthesis with stacked generative adversarial networks. *IEEE transactions on pattern analysis and machine intelligence*, 41(8): 1947–1962.

Zhang, R.; Isola, P.; Efros, A. A.; Shechtman, E.; and Wang, O. 2018b. The unreasonable effectiveness of deep features as a perceptual metric. In *Proceedings of the IEEE conference on computer vision and pattern recognition*, 586–595.

Zhang, Z.; Ma, J.; Zhou, C.; Men, R.; Li, Z.; Ding, M.; Tang, J.; Zhou, J.; and Yang, H. 2021. M6-UFC: Unifying Multi-Modal Controls for Conditional Image Synthesis. *arXiv preprint arXiv:2105.14211*.

Zhou, L.; Du, Y.; and Wu, J. 2021. 3d shape generation and completion through point-voxel diffusion. In *Proceedings of the IEEE/CVF International Conference on Computer Vision*, 5826–5835.

Zhou, M.; Zhou, L.; Wang, S.; Cheng, Y.; Li, L.; Yu, Z.; and Liu, J. 2021. UC2: Universal Cross-lingual Cross-modal Vision-and-Language Pre-training. In *Proceedings of the IEEE/CVF Conference on Computer Vision and Pattern Recognition*, 4155–4165.

Zhuge, M.; Gao, D.; Fan, D.-P.; Jin, L.; Chen, B.; Zhou, H.; Qiu, M.; and Shao, L. 2021. Kaleido-BERT: Vision-Language Pre-training on Fashion Domain. In *Proceedings of the IEEE/CVF Conference on Computer Vision and Pattern Recognition*, 12647–12657.

Appendix A Experimental Settings

A.1 Optimization Details

We use the ABO (Collins et al. 2022) dataset for our experiments. We select items with English textual descriptions and 3D models. The original annotated descriptions do not look like natural language, so we use hand-crafted rules (including removing brand, removing number indicating object size, and moving words of color to the beginning of the sentence) to parse and transform them as close as possible to natural language.
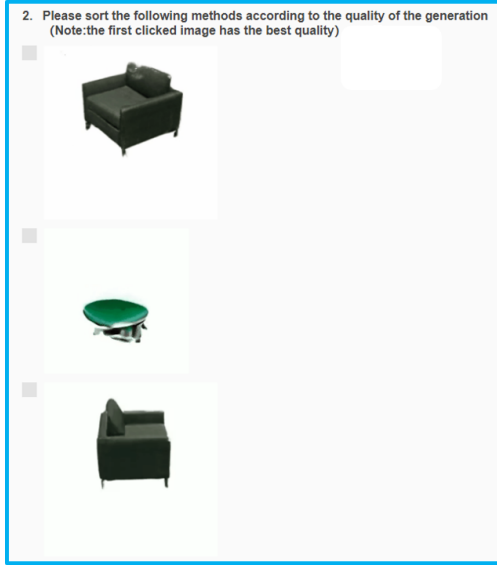
(a) Screenshot for ordering according to object fidelity.

(b) Screenshot for ordering according to caption similarity.

Figure 5: Screenshots of our volunteer questionnaire survey.

We implement our algorithm with Pytorch. All experiments are conducted on servers with 8 Nvidia V100 GPU (32GB) cards and Intel Xeon Platinum 8168 CPU (2.70GHz). Hyperparameters are searched on the validation set.

For our text-to-views generation module, we use the released VQGAN (Esser, Rombach, and Ommer 2021) model as the image tokenizer. The size of the codebook is 1024. The input image size is 256×256 and the image tokenizer transforms the input image as $16 \times 16 = 256$ tokens. The vocabulary size of the BPE tokenizer is 49,408. The maximum length of the caption token sequence is 128. 36 camera poses across different objects are selected. We use a 24-layer Transformer with 8 attention heads. The dimension of each attention head is 64. We use the AdamW optimizer with $\beta_1 = 0.9$, $\beta_2 = 0.96$ to train 20 epochs with batch size 768. The initial learning rate is set as 1e-3 and decayed with a cosine annealing scheduler. The whole optimization process takes about 12 hours with 32 Nvidia V100 GPUs (32 GB).

For our views-to-3D generation module, the input image size is 256×256. We use the Adam optimizer to train 100 epochs with the learning rate 1e-4 and randomly select 9 out of 36 views for training at each training step. During the training stage, We use a batch size of 8 objects and 128 rays per object. To avoid sampling invalid rays and improve optimization efficiency, we sample rays in the bounding box surrounding the object for the first 20 epochs. The bounding box is removed from 20 to 100 epochs to avoid background artifacts. Our views-to-3D generation module takes almost 1 day to train on 8 Nvidia V100 GPUs (32GB).

A.2 Human Study

Figure 5 shows the screenshots of our human study (volunteer questionnaire survey). The volunteers are asked to sort the results of different methods in terms of object fidelity (including view fidelity and consistency among different views) and caption similarity (semantic similarity between input caption and the generated 3D object). 94 effective questionnaires are collected eventually. The average rank of different volunteers is used as the final score.

Appendix B More Experimental Results

B.1 Comparison Against Baselines

We compare our 3D-TOGO model against two baselines: text-to-views generation module + NeRF (Mildenhall et al. 2020) (called text-NeRF) and Dreamfields (Jain et al. 2022). As both text-NeRF and Dreamfields require training an individual network for each given natural language description, we randomly select 12 text descriptions from our test set as the input captions. For Dreamfields, we reduce the weight of transmittance loss, extend the duration of target transmittance annealing, and use the prompt engineering "a 3d render of furniture" for some input texts to get better results. Table 5 lists the selected text descriptions. In the main text, we show quantitative results of the first 6 texts, the results of the remaining 6 texts are shown in Table 6. In the main text, we show qualitative results of the first 2 texts, the results of the rest 10 texts are shown in Figure 6.

Table 5: Text descriptions used for comparison against baselines

TextId	Text descriptions
text1	Driftwood Leather Ottoman
text2	Hunter Green Low Back Modern Accent Chair
text3	Cream Herringbone Queen Headboard
text4	Tan Tufted Sofa
text5	Light Grey with White Whipstitch Edge Decorative Throw Pillow
text6	Blue Geometric Area Rug
text7	Passion Pink Old World Vintage Persian Area Rug
text8	Charcoal Leather Loveseat
text9	Linen Fabric Slipcover Sofa Couch
text10	Pewter Marin Studded Sofa
text11	Ivory, Grey French Laundry Stripe Decorative Throw Pillow
text12	Platinum Black Mid-Century Tufted Customizable Daybed Sofa

Table 6: Quantitative comparison against text-NeRF (short for text-to-views generation + NeRF(Mildenhall et al. 2020)) and Dreamfields (Jain et al. 2022).

Metric	Method	text7	text8	text9	text10	text11	text12	12 Texts Avg.
PSNR ↑	text-NeRF	16.33	19.56	20.09	19.17	13.28	0.58	14.04
	Ours	**28.74**	**23.81**	**26.15**	**20.71**	**26.63**	**29.45**	**24.98**
SSIM ↑	text-NeRF	0.843	0.866	0.887	0.839	0.702	0.001	0.636
	Ours	**0.873**	**0.897**	**0.928**	**0.865**	**0.889**	**0.952**	**0.900**
LPIPS ↓	text-NeRF	0.138	0.110	0.109	0.137	0.379	0.482	0.239
	Ours	**0.099**	**0.015**	**0.084**	**0.122**	**0.092**	**0.062**	**0.092**
CLIP- Score ↑	Dreamfields	18.63	18.16	16.39	19.44	20.11	16.56	18.40
	text-NeRF	18.05	**24.70**	13.97	22.22	13.03	11.61	18.38
	Ours	**24.63**	24.12	**15.71**	**22.47**	**23.00**	**21.42**	**22.84**
Object Fidelity ↓	Dreamfields	2.97	2.95	3.00	2.83	2.38	1.99	2.63
	text-NeRF	1.94	**1.52**	1.97	2.08	2.56	2.94	2.27
	Ours	**1.09**	1.54	**1.03**	**1.08**	**1.05**	**1.07**	**1.11**
Caption Similarity ↓	Dreamfields	2.96	2.91	2.92	2.87	2.47	2.02	2.64
	text-NeRF	1.91	**1.51**	2.04	2.07	2.49	2.94	2.25
	Ours	**1.13**	1.57	**1.04**	**1.05**	**1.03**	**1.04**	**1.11**

We also compare our 3D-TOGO model against CLIP-Forge(Sanghi et al. 2022). As CLIP-Forge generates 3D objects without color and texture, we only conduct the qualitative comparison. Figure 7 shows the qualitative results of CLIP-forge on the 12 text descriptions in Table 5. As we can see, CLIP-forge can generate desired 3D shapes for ottoman, chair, loveseat, and sofa categories, while fails for pillow, headboard, and rug categories. Compared with CLIP-Forge, our 3D-TOGO can generate high-quality realistic 3D objects with color and rich textures on all these input captions.

B.2 Text-Guided 3D Object Generation

Figure 8 and Figure 9 show more cross-category generation results of our 3D-TOGO model. In the supplementary materials, we also provide explanatory supplementary videos of the generated text-matched 3D objects. These videos include renderings where the camera is moved around the object.

To further demonstrate the superiority of our 3D-TOGO regarding the shape and color control, we conduct qualitative comparison experiments for 3D-TOGO and CLIP-Forge

with changed color and shape. Figure 10 and Figure 11 show more results of generating 3D objects with controlled color and shape respectively. Figure 12 shows the qualitative results of CLIP-forge for various color and shape. As displayed in Figures 10, 11, 12, CLIP-forge fails to control the color and shape of generated 3D objects, while our 3D-TOGO can generating realistic text-matched 3D objects.

Appendix C   Ablation study

As mentioned in the main text, in this section, we study the effectiveness of different objectives mentioned in the 3D-TOGO model on the quality of generated views from the text-to-views generation module and 3D objects from the views-to-3D generation module respectively. For quantitative comparison of the quality of generated views, we adopt metrics including FID (Heusel et al. 2017), KID (Bińkowski et al. 2018), CLIP score and consistency error. FID and KID measure the distance between feature distributions of the real views and generated views. The lower FID and KID, the better view fidelity. CLIP score measures the semantic

Table 7: Ablation study of our 2D view-consistent text-to-image generation module. '*prior*' indicates *prior*-guidance, 'contrastive' indicated view contrastive learning, 'caption' indicates caption-guidance and 'L1' indicates pixel-level L1 loss.

prior	contrastive	caption	L1	FID ↓	KID (* 1e-3) ↓	CLIP-score ↑	consistency-error ↓
				15.72	3.76	20.58	9.47
✓				15.44	3.29	20.62	8.88
	✓			15.13	2.95	20.67	9.17
		✓		14.43	2.80	21.23	9.23
			✓	15.52	3.63	20.59	9.35
✓	✓			15.43	2.99	20.63	8.61
✓		✓		14.99	2.93	**21.20**	8.81
✓		✓	✓	**14.70**	2.77	**21.20**	8.74
✓	✓	✓	✓	**14.70**	**2.64**	**21.20**	**8.56**
GT				0	0	22.88	7.55

Table 8: Ablation study of our text-to-views generation module and the effectiveness on 3D object generation measured by CLIP-score. '*prior*', 'contrastive', 'caption' and 'L1' indicates *prior*-guidance, view contrastive learning, caption-guidance and pixel-level L1 loss respectively.

prior	contrastive	caption	L1	Chair	Sofa	Lamp	Planter	Pillow
				20.44	20.25	18.32	23.57	21.21
✓				20.94	21.03	19.06	23.87	21.48
	✓			20.38	19.91	18.73	23.65	20.90
		✓		20.78	20.36	19.12	23.96	21.43
			✓	20.51	20.31	18.70	23.50	21.50
✓	✓			21.09	20.94	19.71	23.76	21.65
✓		✓		21.60	21.29	19.86	24.02	22.13
✓		✓	✓	21.57	21.46	19.20	23.91	21.90
✓	✓	✓	✓	**21.75**	**21.51**	**20.38**	**24.14**	**21.97**

prior	contrastive	caption	L1	Tools	Bed	Dehumidifier	Light Fixture	Exercise Mat
				15.12	19.60	17.62	15.79	21.77
✓				15.34	19.94	17.33	16.00	22.69
	✓			15.09	18.94	17.83	16.40	22.40
		✓		15.45	19.05	18.23	16.85	23.08
			✓	15.40	19.50	16.88	15.59	22.11
✓	✓			16.73	20.24	17.48	16.33	22.80
✓		✓		15.19	20.48	18.86	16.82	23.51
✓		✓	✓	15.43	20.21	18.85	15.61	23.32
✓	✓	✓	✓	**19.28**	**20.17**	**19.77**	**17.29**	**23.97**

prior	contrastive	caption	L1	Home	Instrument	Healthcare	Multiport Hub	Recording Equipment
				17.10	15.07	21.96	16.88	14.38
✓				17.55	16.07	22.60	17.19	16.74
	✓			17.43	15.02	21.73	16.83	16.62
		✓		17.14	13.78	23.54	17.00	16.90
			✓	17.28	15.21	21.99	16.85	15.46
✓	✓			17.53	16.35	22.62	17.06	16.34
✓		✓		17.58	16.75	23.17	16.94	17.39
✓		✓	✓	17.48	17.55	23.90	17.23	18.05
✓	✓	✓	✓	**18.10**	**18.25**	**23.98**	**17.39**	**18.67**

prior	contrastive	caption	L1	Ottoman	Cabinet	Headboard	Stool Seating	**All Categiries Avg.**
				24.34	19.02	17.59	22.04	19.91
✓				25.35	20.05	17.62	22.39	20.50
	✓			24.28	19.23	17.43	21.96	19.79
		✓		24.58	19.26	17.99	22.39	20.14
			✓	24.64	19.21	17.38	22.08	19.99
✓	✓			25.21	20.14	17.60	22.47	20.54
✓		✓		25.37	20.37	18.18	22.58	20.90
✓		✓	✓	25.48	20.24	18.17	22.59	20.93
✓	✓	✓	✓	**25.64**	**20.61**	**18.26**	**22.86**	**21.01**

similarity between the input caption and the generated views and is the higher the better. Consistency error measures the average L2 error between views of adjacent camera poses and reflects view consistency to some degree. The lower the consistency error, the better view consistency.

C.1 View Generation Quality

Table 7 shows the quantitative results of our text-to-views generation module. As we can see, $prior$-guidance improves the consistency-error from 9.47 to 8.88, and view contrastive learning further improves it to 8.61, indicating both of these two improvements contribute to improving view-consistency. Besides, our complete text-to-views generation module achieves the best consistency-error of 8.56. Besides, $prior$-guidance also decreases FID and KID, indicating improved view fidelity. This indicates that the extra information $prior$-guidance provided not only improves view-consistency, but also helps the task of view generation. Caption-guidance improves the CLIP-score from 20.62 to 21.22, meanwhile decreasing FID from 15.44 to 14.99. We deem that this improvement stems from the pixel-level supervision signal from CLIP loss compensating for the original token-level training signals. Besides the CLIP loss, the pixel-level $L1$ loss further improves the view fidelity and lowers the FID. We obtain our best text-to-views generation module by integrating all these techniques.

C.2 3D Object Generation Quality

Table 8 reports the CLIP-scores of our views-to-3D generation module for more object categories. As we can see, 3D object generation based on the results of our complete text-to-views generation module achieves the best CLIP-score in all shown categories and achieves the best average CLIP-score among all categories of the ABO test set. Compared with contrastive learning, caption guidance and pixel-level L1 loss, the prior guidance has the largest performance improvement for our 3D-TOGO model. This is because it can greatly improve consistency among the images generated by the text-to-views modules.

C.3 Qualitative Comparison for $Prior$-guidance and View contrastive learning

Figure 13 illustrates the effectiveness of $prior$-guidance and view contrastive learning on improving view consistency. For views from the text-to-views generation module, we can see that compared with the base module, $prior$-guidance improves the view-consistency of 2D generated images, but as the rank of camera pose increases, view-consistency may decrease in more complicated cases due to some accumulated error (see the left 4th image in the 3rd row). Further with the view contrastive learning, the long-range view-consistency is improved.

C.4 Qualitative Comparison for Caption Loss

Figure 14 shows the comparison between results without caption loss and with caption loss. As we can see, without the caption loss, the model swing between bed and nightstand. On the contrary, with the caption loss, the model consistently generates a nightstand.

C.5 Qualitative Comparison for L1 Loss

Figure 15 shows the comparison between results without L1 loss and with L1 loss. As we can see, with the L1 loss, a finer-grained training signal, the model can generate results with better details.

C.6 Multi-views generated by text-to-views module

It is challenging to generate view-consistent multi-view images from text. Although we improve the consistency among different views by the prior guidance and view contrastive learning, the consistency error of the multi-view images generated by the text-to-views module is still large than that of the ground-truth images as shown in Table 2 of the main text. Figure 16 shows the multi-views generated by the text-to-views module for the 12 selected texts. For those views with high view consistency, a NeRF model can be trained from scratch and regularization is a great idea to improve the quality of the generated 3D objects. However, for those views with small inconsistent contents, such as Headboard and Rug, direct training on these views produces artifacts or even leads to the collapse of the trained model. For the views-to-3D module, we learn scene prior from the ground-truth images and it does not require test-time optimization. Therefore, it can synthesis high-quality 3D objects from the generated views with good efficiency even if there are some small inconsistent contents among the generated views.

C.7 Generalization of views-to-3D module

As mentioned above, the views-to-3D module learns a scene prior from the training data, so it has the ability to generalize to unseen categories. Figure 17 shows generalization results of the views-to-3D module. Specifically, we train the views-to-3D module on the sofa categories and test the trained model on 8 randomly selected unseen categories. As we can see, the views-to-3D module can obtain good results on the unseen categories.

C.8 Nearest Neighbor Analysis

We perform nearest neighbor analysis to check whether our model purely memorizes the training data or can generate new objects. Specifically, for each generated object, we calculate the total L2 distance among 4 views between it and each object in the training set and check the closest one. Figure 18 and 19 shows the results. As we can see, our model does not just memorize the training set, but can generate new objects with different shape and different color according to the input text.

Appendix D Discussion

D.1 Metrics

Like text-to-image generation, better quantitative metrics are needed for text-guided 3D object generation. NeRF (Mildenhall et al. 2020) and PixelNeRF (Yu et al. 2021) use metrics including PSNR, SSIM and LPIPS to measure the average distance between the synthesized novel views and the ground truth views. This is reasonable because their

goal is to **reconstruct** the 3D object from some collected views. However, in this paper, we aim to generate 3D objects from the input caption, without any collected views. In many cases, our model generates 3D objects that are semantically aligned with the input caption but with views different from the 'ground truth' views. So, it is unreasonable to use these metrics to measure the performance of our model. We use these metrics in the comparison against text-NeRF following the practice in NeRF. We use CLIP-score in the comparison against baseline methods and the ablation study. CLIP-score measures the semantic similarity between the rendered views from the generated 3D objects and the input caption. Besides, the low image quality also yields a low CLIP-score, so it also reflects the visual fidelity of the generated 3D objects. As quantitative metrics are not perfect currently, we also conduct human studies to compare our 3D-TOGO models against baseline methods.

D.2   3D-TOGO VS DALLE and CogView

Using an auto-regressive Transformer for text-to-image generation is commonly used in DALLE(Ramesh et al. 2021), Cogview(Ding et al. 2021) due to its effectiveness in capturing cross-modal correspondence. Based on this progress, we introduce techniques including Pixel-Level Supervision, Caption-Guidance, prior-Guidance and View Contrastive Learning to better generate consistent multi-view images of an object, which is not considered in previous works and is critical for text-to-3D generation. Besides, DALLE and Cogview focus on the single-view image generation from the input text, while 3D-TOGO focuses on the multi-view images generation from the input text.

D.3   3D-TOGO VS PixelNeRF

PixelNeRF(Yu et al. 2021) is a framework to learn a scene prior for reconstructing NeRF representations from one or a few images. In our method, we introduce PixelNeRF as our views-to-3D module. The reasons we choose PixelNeRF as the backbone of views-to-3D module are three-fold:

- PixelNeRF aims to learn a scene prior instead of remembering the training dataset, allowing it to be used for generating objects across different categories or unseen categories. To demonstrate the ability of generalizing to unseen categories, we train the views-to-3D module on the sofa category and test the trained model on 8 randomly selected unseen categories. As shown in Figure 17, the views-to-3D module can obtain good results on the unseen categories.

- PixelNeRF is trained across multiple scenes and does not requires test-time optimization, which improves the flexibility for generating 3D objects from text.

- PixelNeRF can predict a neural radiance field representation from a spare set of views, which reduces the cost of text-to-views module.

PixelNeRF is designed for predicting a Neural Radiance Field representation from few images. In this paper, our task is the cross-category 3D object generation from text.

D.4   3D-TOGO VS DreamFields

Dreamfields(Jain et al. 2022) optimizes a Neural Radiance Field by minimizing the distance between the rendered images and the input text with a pre-trained CLIP model. The pipeline of Dreamfields is completely different from the proposed method. Dreamfields is a one stage solution that goes from text directly to NeRF, while the proposed method is a two stage solution. In the proposed method, we first generate consistent multi-view images of an object and then reconstruct 3D object from these generated consistent multi-view images. The rendered images of Dreamfields are rendered by sampling different camera poses, while the multi-view images of the proposed method are directly generated from the input text. Inherited from NeRF(Mildenhall et al. 2020), Dreamfields requires training a separate model for each input text, which usually takes more than 1 hour with 8 TPU cores. Compared with Dreamfields, the proposed method has an efficient generation process. Besides, hyper-parameters of Dreamfields are manually tuned on the COCO dataset. Given a caption of the ABO dataset, it is difficult to do such hyperparameter tuning. Another advantage of 3D-TOGO is that it can generate more realistic 3D objects.

D.5   3D-TOGO VS CLIP-Mesh and DreamFusion

CLIP-Mesh (Khalid et al. 2022b) and DreamFusion (Poole et al. 2022) seem to produce amazing and promising 3D objects. However, both of them require training a separate model for each input text on the fly, which is time-consuming and limits its practical application. Compared with them, 3D-TOGO is a generic model and does not require inference time optimization. 3D-TOGO can generate a 3D object within 2 minutes, while CLIP-Mesh and DreamFusion require 50 minutes and 3 hours respectively.

Appendix E   Failure cases

Figure 20 shows some failure cases of our model. If the input text is completely out of the distribution of ABO, it might fail to generate desired text-matched 3D objects. In the experiments, one interesting thing is that our 3D-TOGO can generate 3D objects of unseen categories by using prompt engineering "a painting of" as shown in Figure 21. We believe the generalization ability of our 3D-TOGO model can be scaled by pretraining on more text-image samples and using a larger generation model. CO3D(Reizenstein et al. 2021), containing a total of 1.5 million frames from nearly 19,000 videos capturing objects from 50 MS-COCO categories, is one that could be used to improve the ability of our 3D-TOGO model. Besides, it is possible to improve the generalization of the proposed method with single-view images of objects, which are easily collected. In some cases, 3D-TOGO could be unable to control the shape of generated 3D objects, which can be solved by using repetition words describing 3D shapes.

Appendix F   Conclusion

F.1   Potential negative social impact

Our method has no ethical risk on dataset usage and privacy violation since all the benchmarks are publicly avail-

able. Besides, our method offers a new way to generate 3D objects and we do not expect a negative social impact as the generated 3D objects are generated with textual guidance. If the training data on some sensitive categories is available, the proposed method could be misused for generating real 3D humans or weapons. Such misuse of 3D object generation from text techniques poses a societal threat, and we do not condone using our work with the intent of spreading misinformation or tarnishing reputation.

F.2 Limitations and future works

If the input text is completely out of the distribution of ABO, it might fail to generate desired text-matched 3D objects. In the further, we plan to improve the generalization of the proposed method with single view images of objects, which are easily collected. Besides, we will apply our 3D-TOGO model to datasets from other domains, such as humans.
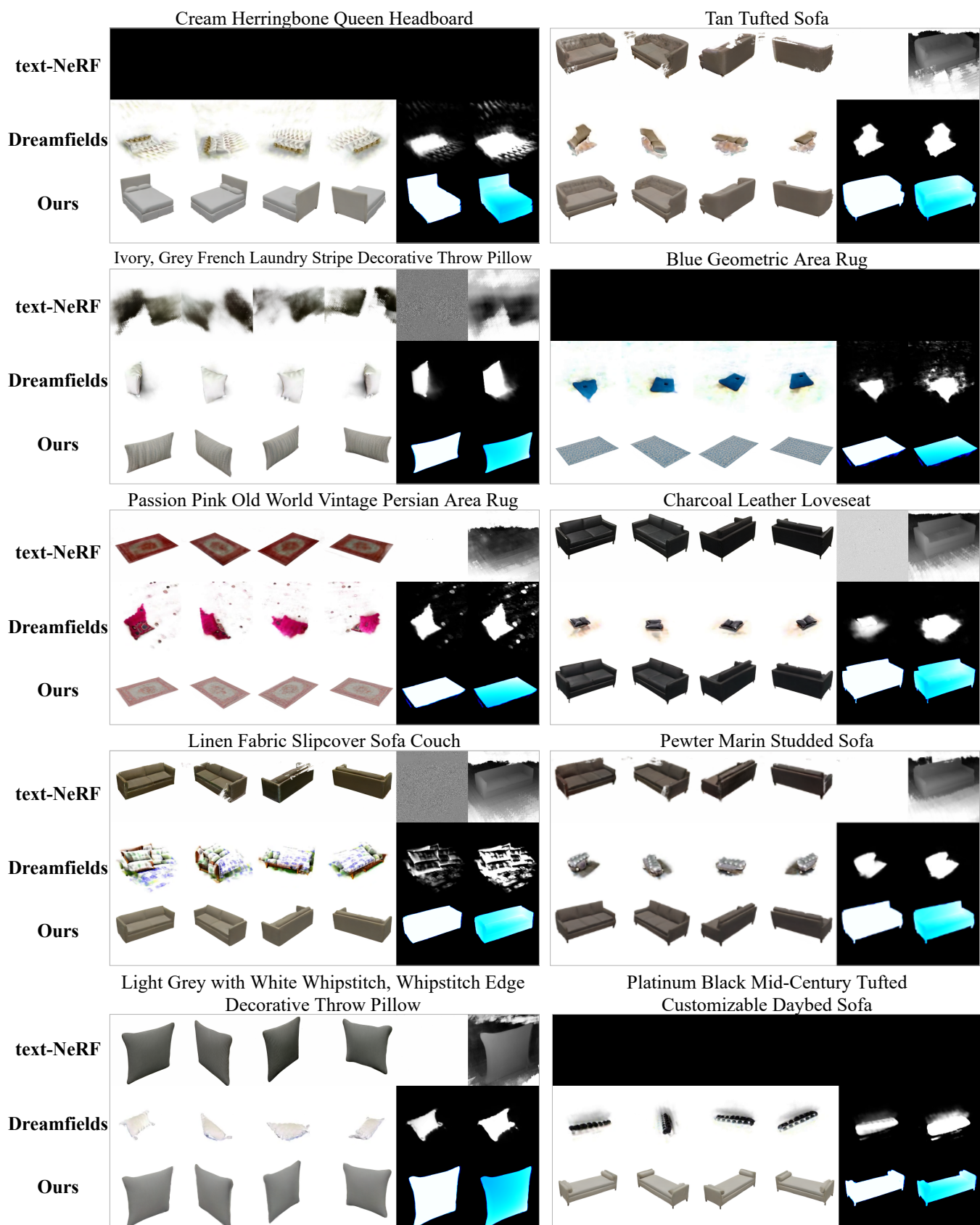
Figure 6: Visual comparison against two baseline methods. For each subfigure, the textual title is the input caption, and the first 4 images are rendered novel views of the generated 3D object while the last two images are transmittance and depth from the first view respectively.

Driftwood Leather Ottoman
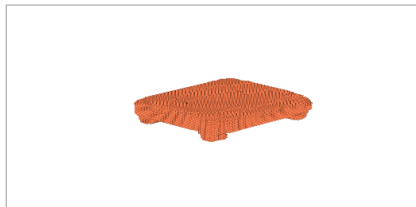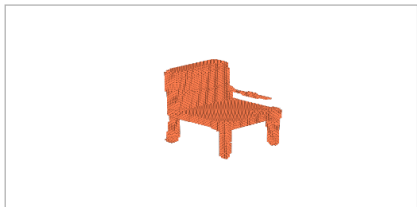
Hunter Green Low Back Modern Accent Chair
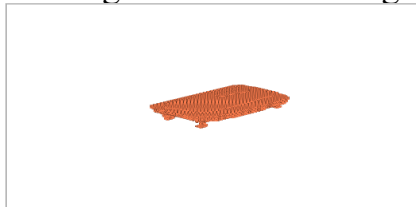
Cream Herringbone Queen Headboard

Tan Tufted Sofa
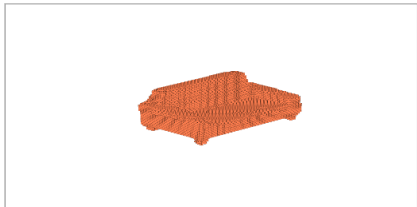
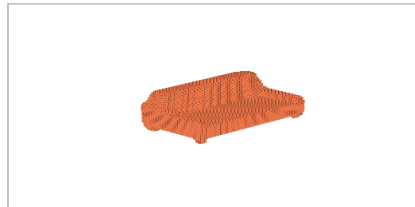Ivory, Grey French Laundry Stripe Decorative Throw Pillow
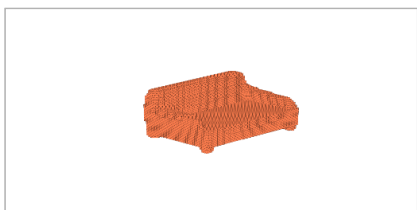
Blue Geometric Area Rug
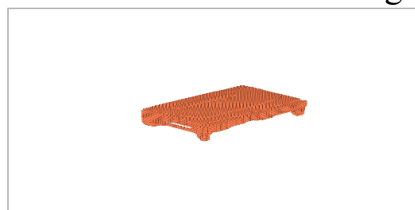
Passion Pink Old World Vintage Persian Area Rug

Charcoal Leather Loveseat

Linen Fabric Slipcover Sofa Couch

Pewter Marin Studded Sofa
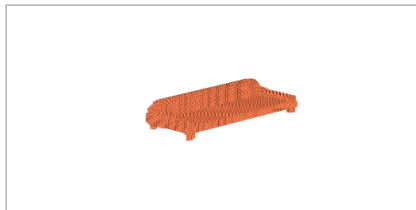
Light Grey with White Whipstitch, Whipstitch Edge Decorative Throw Pillow
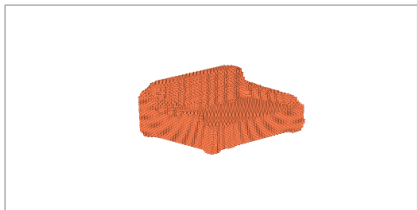
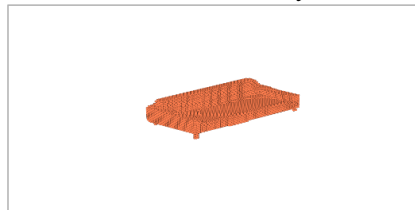Platinum Black Mid-Century Tufted Customizable Daybed Sofa

Figure 7: Qualitative results of CLIP-forge(Sanghi et al. 2022) on 12 texts in Table 5.
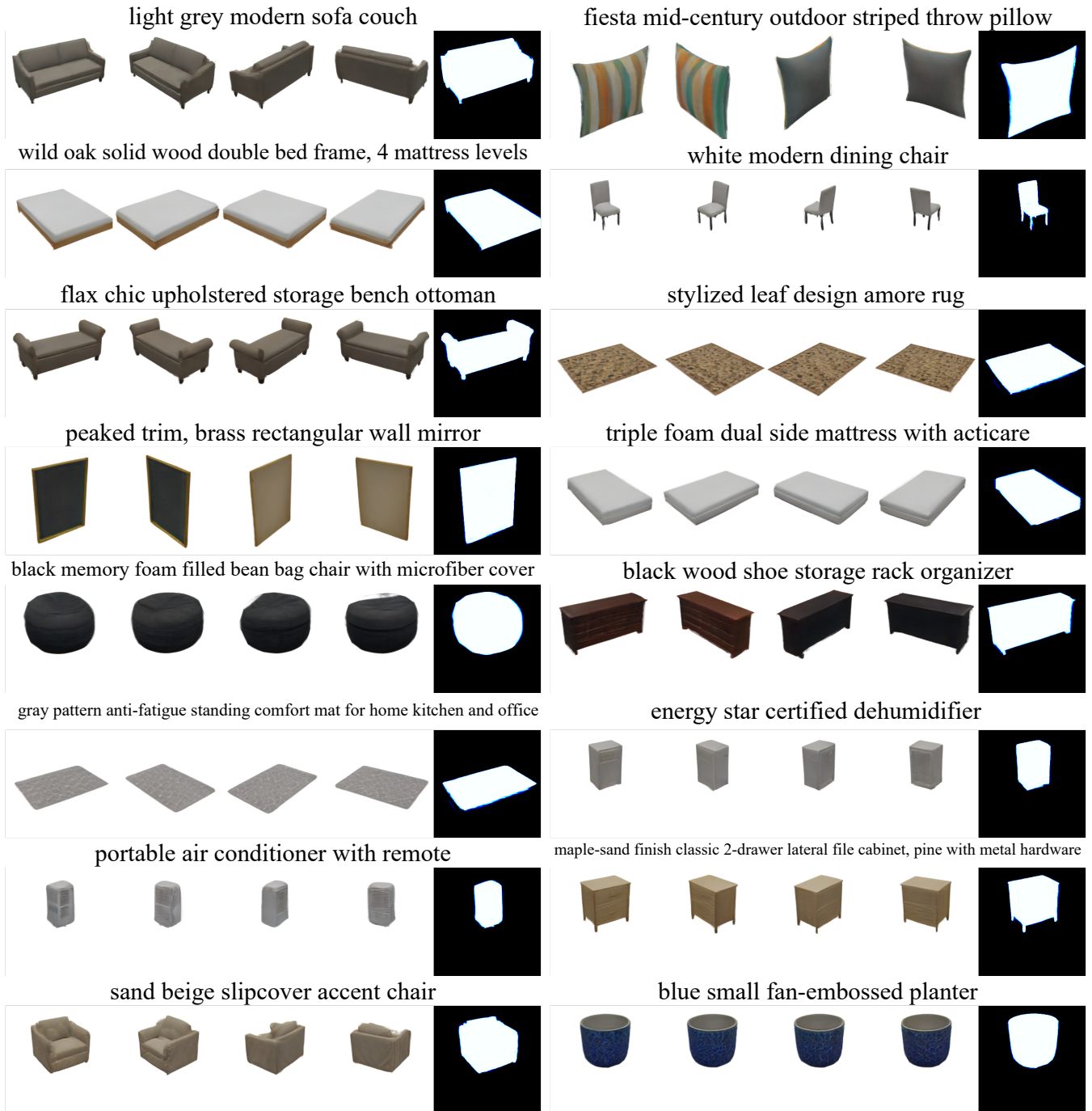
Figure 8: Generation results of our proposed 3D-TOGO model. For each case, we show the input caption, 4 rendered novel views of the generated 3D object and the transmittance from the first view.
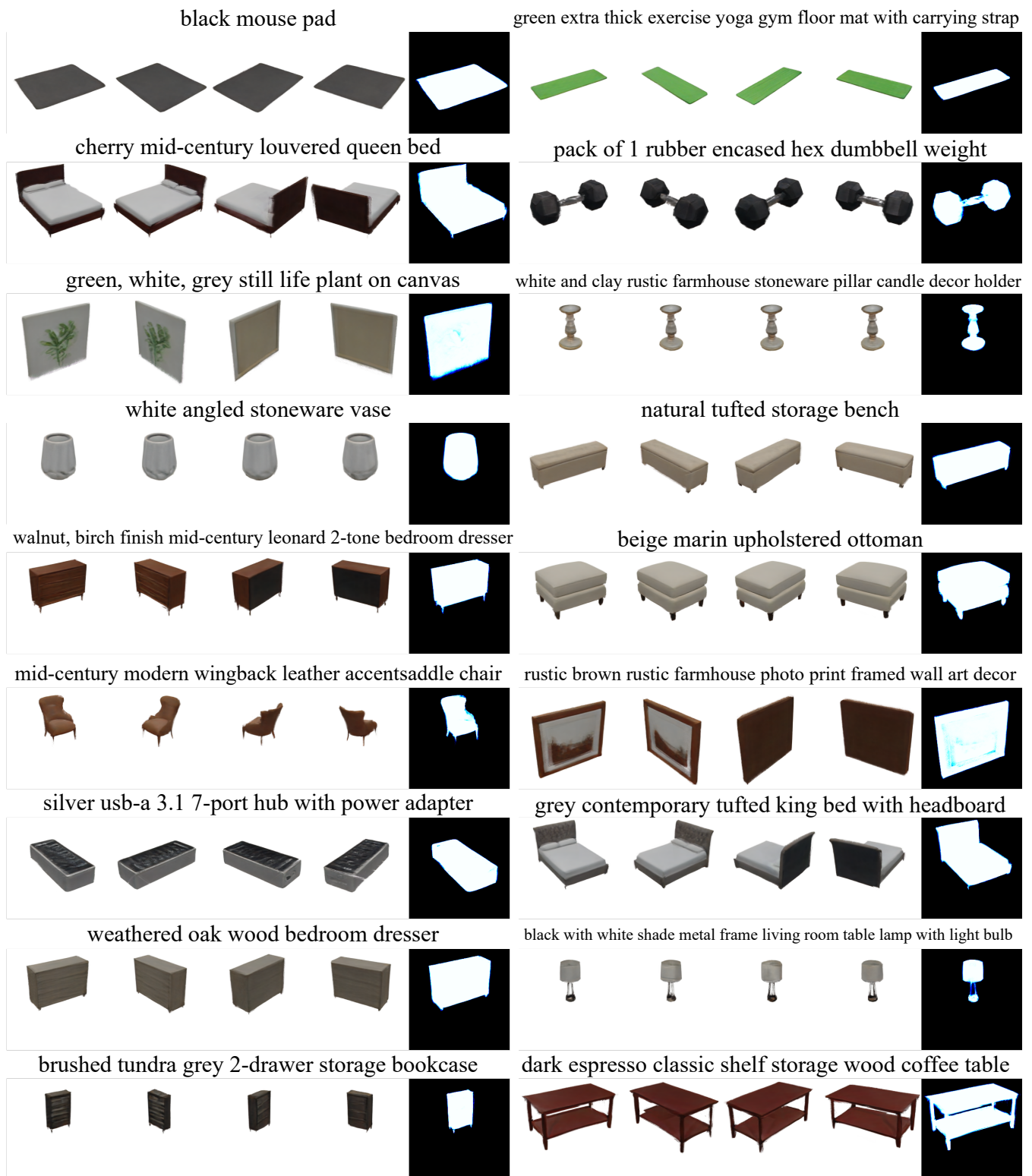
black mouse pad

green extra thick exercise yoga gym floor mat with carrying strap

cherry mid-century louvered queen bed

pack of 1 rubber encased hex dumbbell weight

green, white, grey still life plant on canvas

white and clay rustic farmhouse stoneware pillar candle decor holder

white angled stoneware vase

natural tufted storage bench

walnut, birch finish mid-century leonard 2-tone bedroom dresser

beige marin upholstered ottoman

mid-century modern wingback leather accentsaddle chair

rustic brown rustic farmhouse photo print framed wall art decor

silver usb-a 3.1 7-port hub with power adapter

grey contemporary tufted king bed with headboard

weathered oak wood bedroom dresser

black with white shade metal frame living room table lamp with light bulb

brushed tundra grey 2-drawer storage bookcase

dark espresso classic shelf storage wood coffee table

Figure 9: Generation results of our proposed 3D-TOGO model. For each case, we show the input caption, 4 rendered novel views of the generated 3D object and the transmittance from the first view.
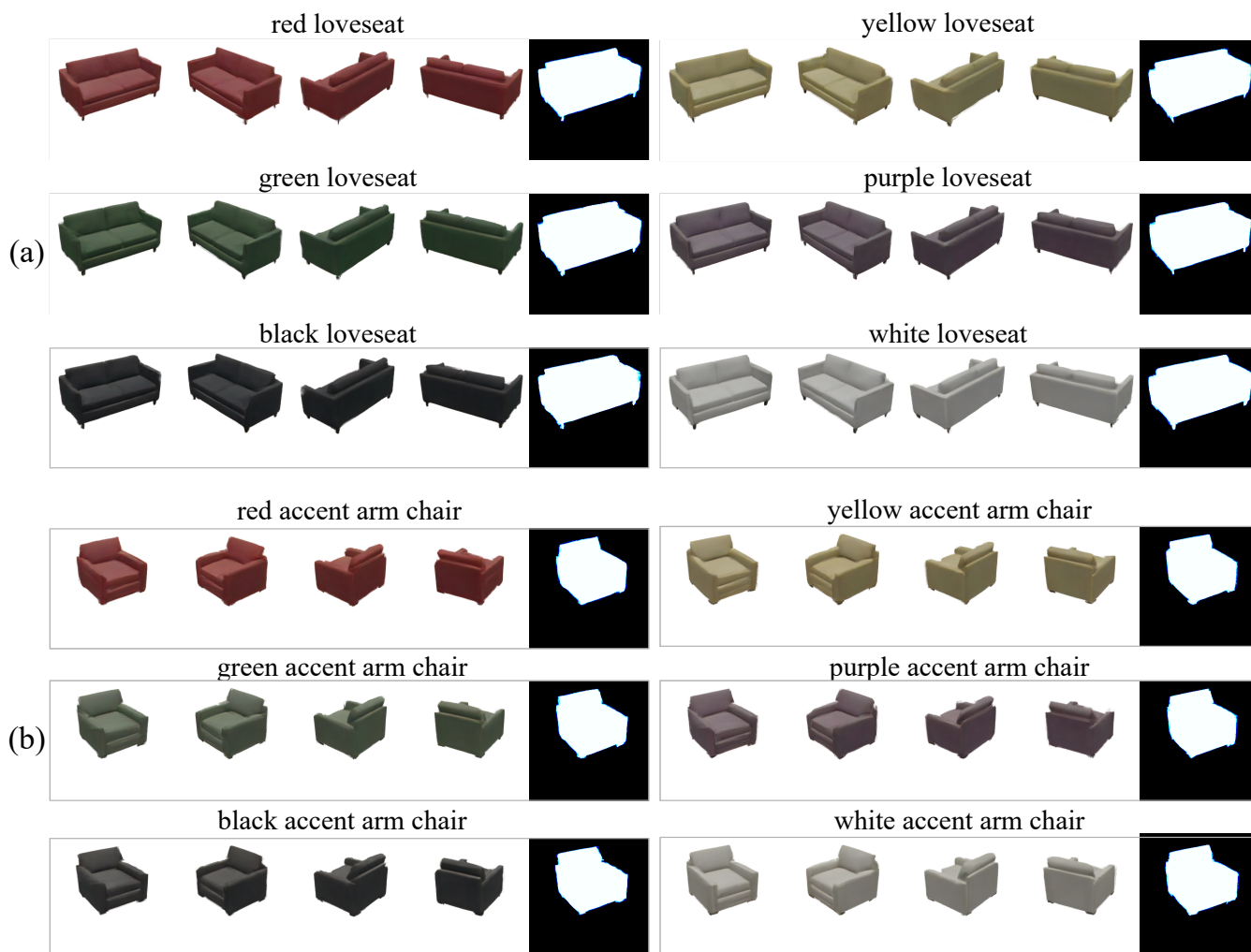
Figure 10: 3D object generation results with controlled color. For each case, we show the input caption, 4 rendered novel views of the generated 3D object and the transmittance from the first view.
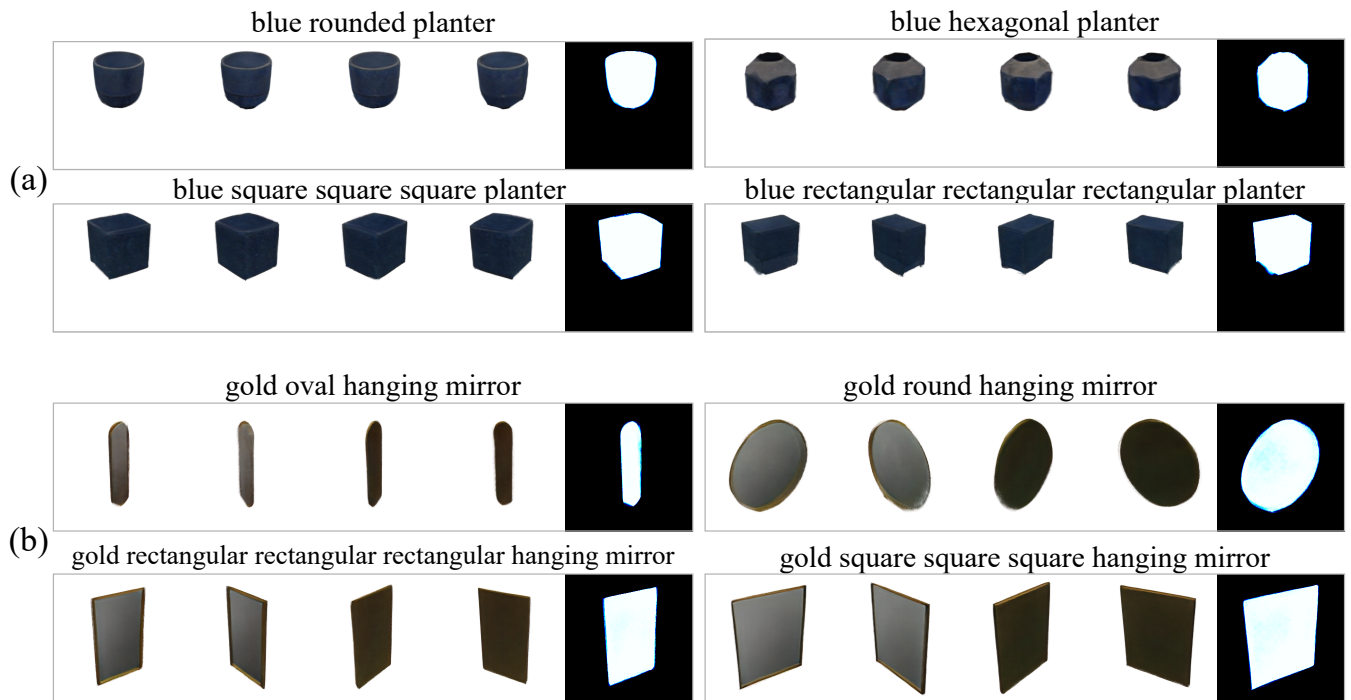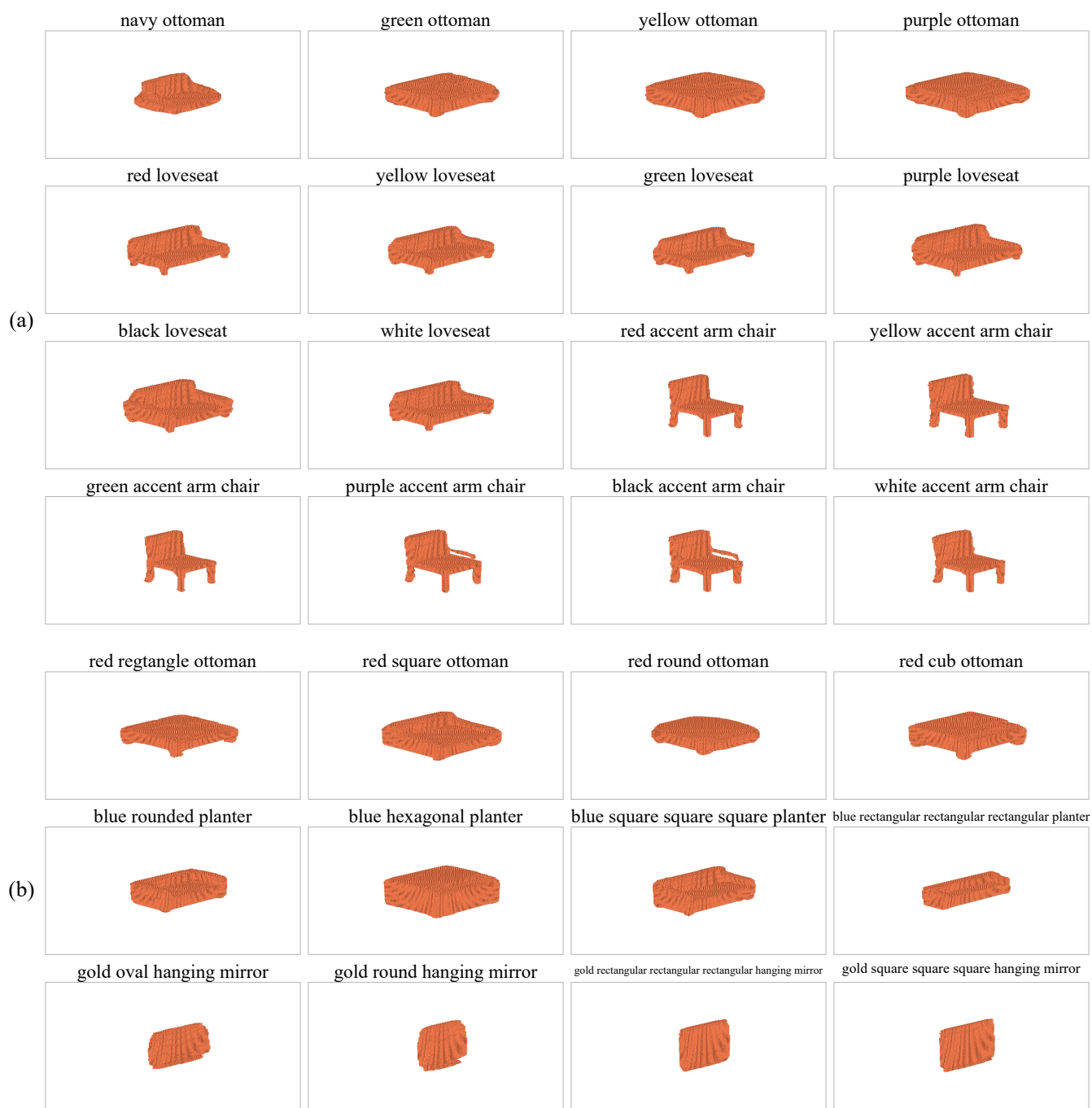
blue rounded planter

blue hexagonal planter

(a)

blue square square square planter

blue rectangular rectangular rectangular planter

gold oval hanging mirror

gold round hanging mirror

(b)

gold rectangular rectangular rectangular hanging mirror

gold square square square hanging mirror

Figure 11: 3D object generation results with controlled shape. For each case, we show the input caption, 4 rendered novel views of the generated 3D object and the transmittance from the first view.

(a)

navy ottoman	green ottoman	yellow ottoman	purple ottoman

red loveseat	yellow loveseat	green loveseat	purple loveseat

black loveseat	white loveseat	red accent arm chair	yellow accent arm chair

green accent arm chair	purple accent arm chair	black accent arm chair	white accent arm chair

(b)

red regtangle ottoman	red square ottoman	red round ottoman	red cub ottoman

blue rounded planter	blue hexagonal planter	blue square square square planter	blue rectangular rectangular rectangular planter

gold oval hanging mirror	gold round hanging mirror	gold rectangular rectangular rectangular hanging mirror	gold square square square hanging mirror

Figure 12: Qualitative results of CLIP-forge(Sanghi et al. 2022) for various color and shape.
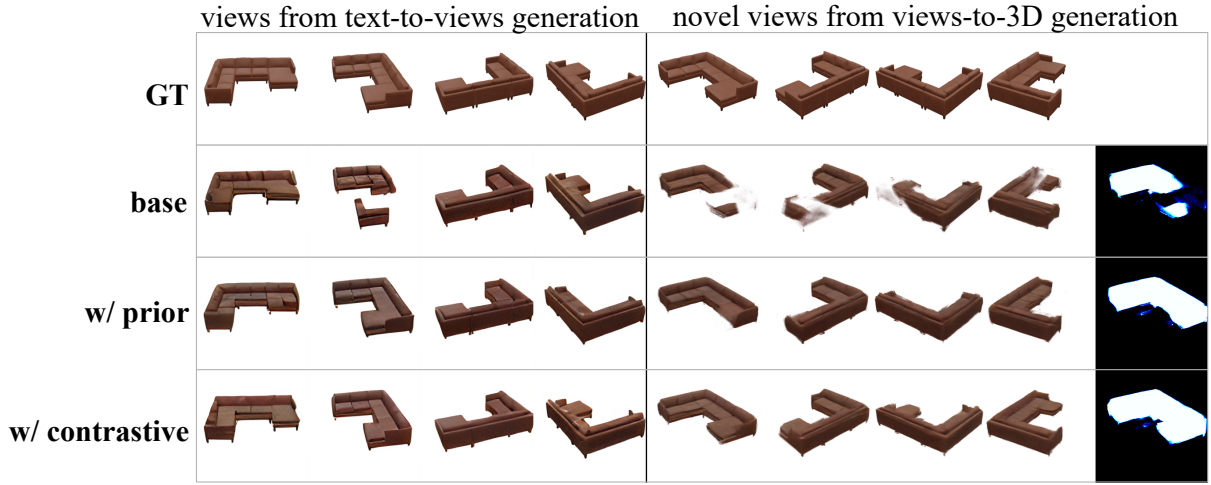
Figure 13: Effectiveness of *prior*-guidance and view contrastive learning. **base**, **prior**, and **contrastive** indicate base text-to-views generation, *prior*-guidance, and view contrastive learning, respectively. The right-most image is the transmittance from the first generated novel view.
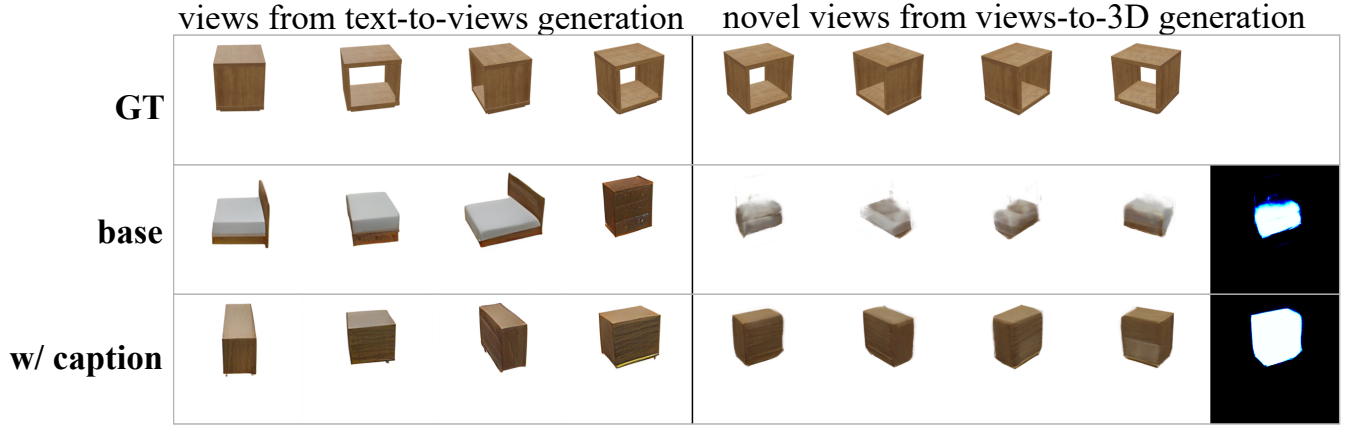
Figure 14: Effectiveness of caption loss. The input caption is 'Oak Finish Industrial Bed side Wood Nightstand'. **base** and **caption** indicate base text-to-views generation and caption-guidance, respectively. The right-most image is the transmittance from the first generated novel view.
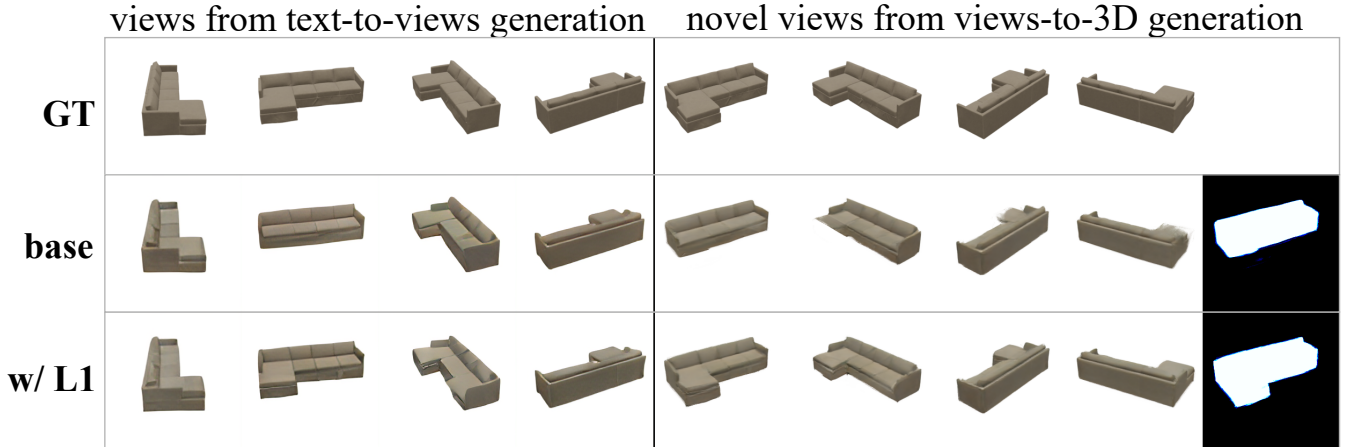
Figure 15: Effectiveness of L1 loss. **base** and **L1** indicate base text-to-views generation and pixel-level L1 loss, respectively. The right-most image is the transmittance from the first generated novel view.

Driftwood Leather Ottoman

Hunter Green Low Back Modern Accent Chair

Cream Herringbone Queen Headboard

Tan Tufted Sofa

Ivory, Grey French Laundry Stripe Decorative Throw Pillow

Blue Geometric Area Rug

Passion Pink Old World Vintage Persian Area Rug

Charcoal Leather Loveseat

Linen Fabric Slipcover Sofa Couch

Pewter Marin Studded Sofa

Light Grey with White Whipstitch, Whipstitch Edge Decorative Throw Pillow

Platinum Black Mid-Century Tufted Customizable Daybed Sofa

Figure 16: Multi-views generated by the text-to-view module for the 12 selected texts.

Figure 17: Generalization of views-to-3D module.

Coral White Tan Round Ceramic Home Decor Flower Vase
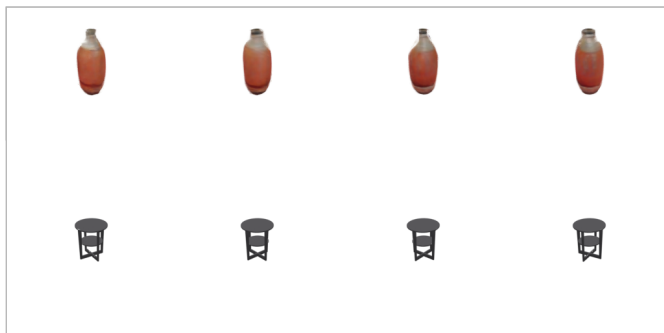
White Angled Stoneware Vase
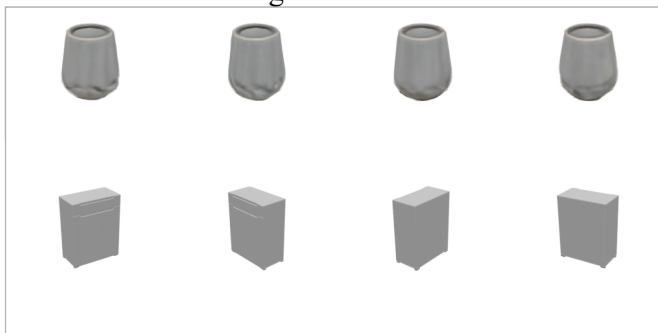
Denim Modern Tweed Lift-Top Storage Ottoman Pouf

Weathered Oak Modern Wood Bedroom Dresser

A8910 Dresser

Gold Leaf mid-Century Modern Oversized Upholstered Square Ottoman

Blue and Black Allie Velvet Industrial Mid-Century Dining Kitchen Chair
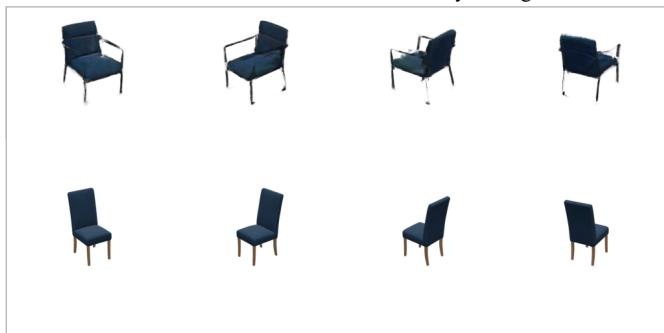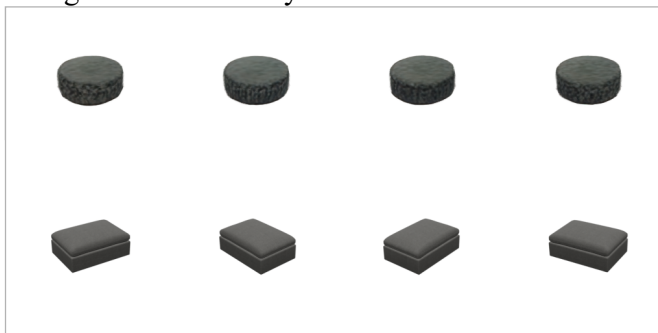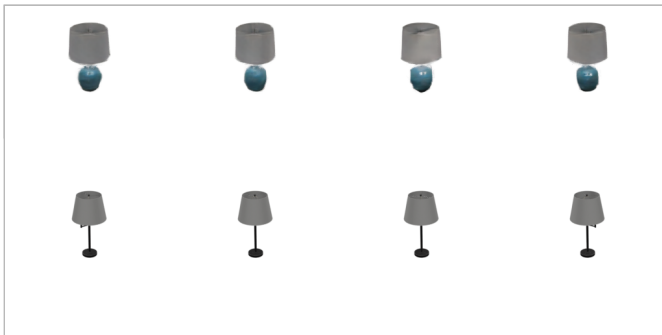

Evergreen Mid-Century Modern Round Tufted Velvet

Figure 18: Nearest neighbor analysis (1). For each object, the title is the input text, the first row of image are views of the generated object, while the second row of image are views of the closest object in the training set.

Cyan Blue Round Ceramic Table Lamp With Light Bulb and White Shade

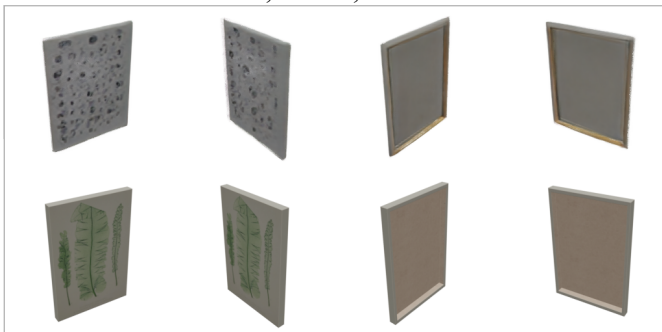**Blue Ink Low Back Modern Right Chaise Sofa Sectional**
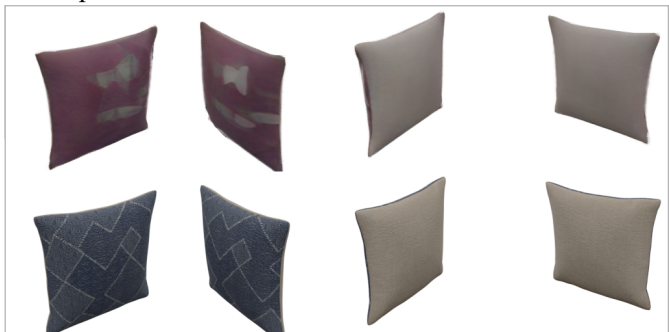
Rouge Red Modern Ottoman

Black Frame Matted Flower X-Ray Photograph

Abstract Black, Silver, Pink Canvas Print

Purple Abstract Geometric Decorative Throw Pillow

Hunter Green Low Back Modern Accent Chair

Fringed, Pink, Blue Medallion Area Rug

Figure 19: Nearest neighbor analysis (2). For each object, the title is the input text, the first row of image are views of the generated object, while the second row of image are views of the closest object in the training set.
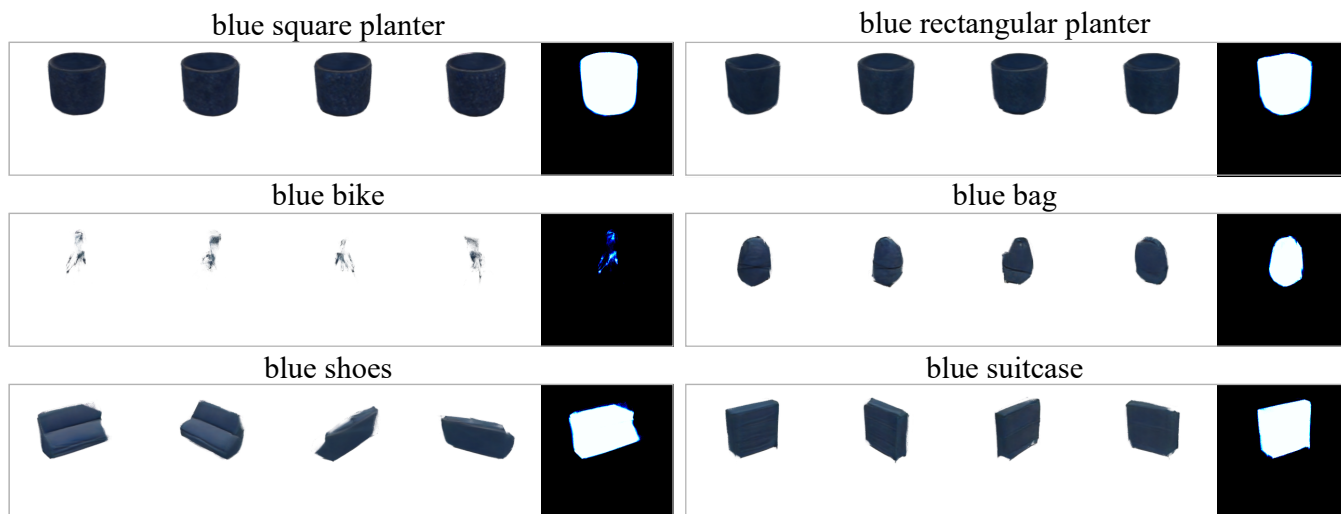
blue square planter

blue rectangular planter

blue bike

blue bag

blue shoes

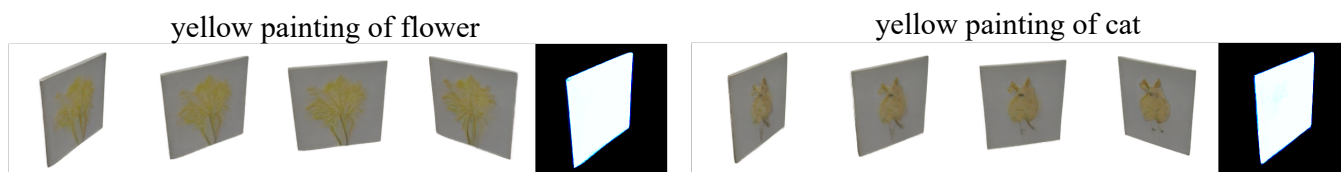blue suitcase

Figure 20: Failure cases.

yellow painting of flower

yellow painting of cat

Figure 21: Flower and cat.